arXiv:2507.07535v1 [cs.NI] 10 Jul 2025

A Fragmentation-Aware Adaptive Bilevel Search Framework for Service Mapping in Computing Power Networks

Jingzhao Xie, Zhenglian Li, Gang Sun, *Senior Member, IEEE*, Long Luo, *Member, IEEE*, Hongfang Yu, *Senior Member, IEEE*, and Dusit Niyato, *Fellow, IEEE*

***Abstract*—Computing Power Network (CPN) unifies wide-area computing resources through coordinated network control, while cloud-native abstractions enable flexible resource orchestration and on-demand service provisioning atop the elastic infrastructure CPN provides. However, current approaches fall short of fully integrating computing resources via network-enabled coordination as envisioned by CPN. In particular, optimally mapping services to an underlying infrastructure to maximize resource efficiency and service satisfaction remains challenging. To overcome this challenge, we formally define the service mapping problem in CPN, establish its theoretical intractability, and identify key challenges in practical optimization. We propose Adaptive Bilevel Search (ABS), a modular framework featuring (1) graph partitioning-based reformulation to capture variable coupling, (2) a bilevel optimization architecture for efficient global exploration with local optimality guarantees, and (3) fragmentation-aware evaluation for global performance guidance. Implemented using distributed particle swarm optimization, ABS is extensively evaluated across diverse CPN scenarios, consistently outperforming existing approaches. Notably, in complex scenarios, ABS achieves up to 73.2% higher computing resource utilization and a 60.2% higher service acceptance ratio compared to the best-performing baseline.**

***Index Terms*—Computing power network, resource allocation, graph partitioning, bilevel optimization, distributed evolutionary algorithms.**

I. Introduction

THE rapid development of emerging applications—including large-scale AI model training and inference, extended reality (XR) applications, and widespread Internet of Things (IoT) ecosystems—is making network services increasingly complex [1]. These novel services exhibit diverse requirements and dynamic characteristics, consume substantial computing resources, and necessitate flexible, on-demand provisioning across all scenarios [2]. However, in this context, conventional network architecture with dedicated infrastructure struggles to satisfy diverse service requirements and often creates resource silos, leading to resource waste and service dissatisfaction [3]. In response, Computing Power Network (CPN) has emerged, integrating distributed heterogeneous computing resources via the network to form an infrastructure characterized by resource pooling and service elasticity, thereby enabling on-demand resource provisioning across domains [3], [4].

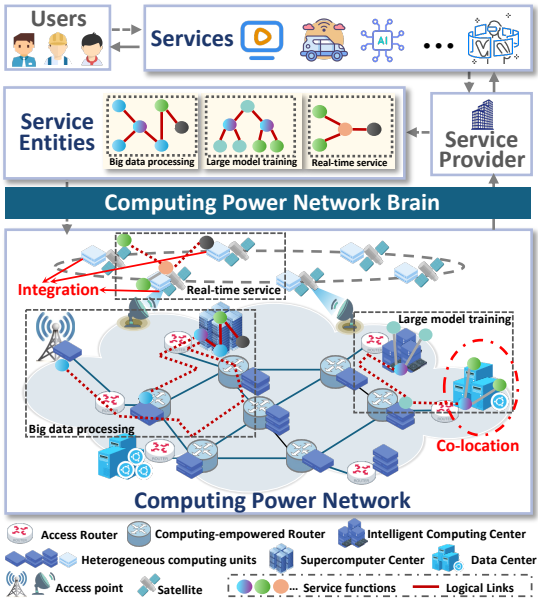


Fig. 1. Conceptual overview of service provisioning and mapping in the CPN environment.

To fully realize the potential of CPN, adopting a cloud-native perspective—characterized by declarative service provisioning and on-demand resource supply—is widely considered essential [3], [5]. The cornerstone of this approach is decoupling services from physical resources and abstracting them into self-contained logical entities known as service entities (SEs). SEs define the essence and behavior of services, typically comprising service functions (SFs) that provide business capabilities, logical links (LLs) transmitting data flows between SFs, and descriptions of business logic and resource requirements [5], [6]. Fig. 1 illustrates this model within CPN: users specify desired service capabilities, which the service provider translates into SEs. These SEs are then dynamically mapped onto the underlying physical infrastructure by the CPN brain [3], which orchestrates resources in accordance with real-time infrastructure conditions. This mapping process enables flexible service provisioning and dynamic resource allocation. More importantly, it lays the foundation for inte-

Jingzhao Xie, Zhenglian Li, Gang Sun, Long Luo, and Hongfang Yu are with University of Electronic Science and Technology of China, Chengdu 611731, China (e-mail: jingzhaoxie@gmail.com; zhenglianli@foxmail.com; {gangsun, llong, yuhf}@uestc.edu.cn).

Dusit Niyato is with College of Computing and Data Science, Nanyang Technological University, Singapore (e-mail: dniyato@ntu.edu.sg).

This work was supported in part by National Natural Science Foundation of China (62394324).

grating distributed computing resources—the central objective of CPN. Specifically, service functions of SEs are mapped to distributed computing nodes and interconnected through logical links, enabling previously isolated resources to collaborate over physical networks as a cohesive system that delivers unified services [7]. Consequently, the network evolves from a mere connectivity medium into a critical enabler for this integration, which in turn requires coordinated control of both SF placement and LL mapping. However, to the best of our knowledge, existing mapping schemes cannot support this coordinated mapping at the necessary level of flexibility and granularity for CPN.

Existing mapping technologies can be broadly categorized into three key schemes: DAG-based models [8]–[10], Service Function Chaining (SFC) [7], [11], [12], and Virtual Network Embedding (VNE) [13]–[17]. Among these, VNE is particularly well-suited for CPN as it enables fine-grained network resource allocation and supports arbitrary SE topologies. In contrast, DAG models merely consider coarse-grained end-to-end connectivity, while SFC is constrained by linear chaining topology. However, traditional VNE abstracts SEs as virtual networks and thus must adhere to network virtualization principles, which enforce a strict one-to-one mapping between virtual nodes and physical nodes [18]–[20]. This restriction precludes SF co-location, forcing all inter-function traffic to traverse the physical network, potentially creating transmission bottlenecks and undermining the CPN objective of network-enabled computing integration. Additionally, it stipulates that the number of SFs per service entity must not exceed the number of computing nodes, which is contradictory to nowadays practical scenarios, where the number of SFs may far exceed the number of available nodes [21]. Furthermore, modern computing platforms now support flexible SF deployment and communication (e.g., container-based co-location and veth pair-based intra-node connections [21]). These advancements enable strategic SF co-location to optimize node utilization [22] and minimize network overhead by alleviating bandwidth bottlenecks through intra-node or intra-domain communication [21], [23]. Nevertheless, there remains a lack of theoretical guidance on how to fully exploit these new capabilities for service mapping in CPN.

In this work, we introduce a Service Entity Mapping (SEM) scheme, which extends traditional VNE by explicitly allowing SF co-location. We focus on developing a general solution framework for SEM problems, aiming at fully leveraging the enabling capabilities of the network to enhance the utilization of computing resources and improve service satisfaction. The main contributions are summarized as follows:

1) We introduce the SEM scheme, a crucial extension of traditional Virtual Network Embedding (VNE), specifically tailored for CPN environments. SEM overcomes the fundamental limitations of VNE in efficiently achieving network-enabled integration of distributed computing resources by allowing explicit optimization of service function co-location.
2) We formulate the online SEM problem as a mathematical model that optimizes long-term system performance by balancing service request satisfaction and computing resource utilization against maintaining network overhead. We formally prove the problem's NP-Hardness, and discuss key challenges for practical optimization, including highly coupled decision variables, exponential solution space explosion, and the breakdown of local metrics.
3) We develop an Adaptive Bilevel Search (ABS) framework for solving the SEM problem. This framework integrates a graph partitioning perspective for generating co-location-aware mapping decisions, a bilevel optimization structure combined with an adaptive feedback mechanism for robust global exploration beyond local optima, and resource fragmentation as a global evaluation mechanism. This comprehensive design empowers ABS to iteratively refine mapping decisions via feedback, bridging global and local optimization and enabling continuous evolution toward overall system optimality.
4) We empirically validate the efficacy and superiority of the proposed ABS framework through extensive simulations. Specifically, we implement ABS by leveraging a distributed particle swarm optimization algorithm. Our comprehensive experimental results demonstrate that ABS significantly outperforms state-of-the-art methods across key performance metrics, including system profit, service request acceptance ratio, and long-term average revenue.

The rest of the paper is organized as follows. Section II reviews related works. Section III formulates the mathematical model of the online SEM problem, analyzes its theoretical and practical difficulties, and provides key solution insights. Section IV proposes the design of the ABS framework and presents its implementation details. Section V discusses the simulation results. Finally, Section VI concludes the paper.

II. Related Work

We present the service mapping schemes and discuss key technologies for service function co-location in CPN environments.

A. Service Mapping Schemes

DAG-based mapping: It models service entities as Directed Acyclic Graphs (DAGs), where nodes represent service functions and edges capture their dependencies [8]. This structure clarifies functional relationships and facilitates efficient mapping of SFs to distributed nodes. For example, Fan et al. [9] studied QoE-oriented task scheduling in distributed networks, proposing a heuristic hierarchical multi-queue algorithm to determine the execution order and mapping of SFs jointly. Goudarzi et al. [10] investigated service mapping in edge and fog computing by modeling SEs as DAGs. To improve adaptability, a distributed deep reinforcement learning (DRL) approach is employed, utilizing parallel actors and aggregated experiences for policy updates. However, DAG-based methods primarily portray logical dependencies, often simplifying network connections as point-to-point channels that only reflect transmission delays [10]. This abstraction overlooks the allocation of intermediate network links, which limits fine-grained coordination between computing and network resources and thus constrains computational integration in network-constrained CPN scenarios.

SFC-based mapping: Service entities are represented as linear function chains, explicitly considering fine-grained network links and corresponding resource requirements between service functions. He et al. [7] addressed heterogeneous resource orchestration in space-air-ground integrated networks by modeling SFC mapping and resource allocation as an MINLP problem, proposing an alternating iterative algorithm. Dong et al. [2] proposed a federated meta-reinforcement learning method for fast, privacy-preserving policy adaptation in SFC-based 6G network slicing, while Zhang et al. [24] introduced a heuristic for joint SFC placement and VNF migration in multi-domain networks. Most of these works do not explore the co-location of service functions. Wang et al. [11] investigated co-location strategies to improve resource utilization and latency and proposed a parallelized SFC deployment algorithm on a CPU+DPU heterogeneous architecture for enhanced flexibility and performance. Nevertheless, the linear chaining model of SFC limits its implementation flexibility to support complex topologies and diverse service requirements, making it less suitable for CPN-oriented service mapping.

VNE-based mapping: Compared to DAG and SFC, the VNE scheme is better suited for service mapping in CPN environments due to its support for both fine-grained network resource allocation and arbitrary SE topologies. Zhang et al. [14] proposed a DRL-based QoS-aware VNE algorithm for space-air-ground-ocean integrated networks, which utilizes K-means clustering to classify each request's QoS requirements and dynamically optimizes mapping strategies for improved resource utilization. Geng et al. [25] proposed GAL-VNE, which combines global reinforcement learning with local one-shot neural prediction. This approach globally optimizes resource allocation across requests and performs mapping efficiently at the local level. Guan et al. [26] addressed multi-dimensional resource fragmentation to optimize edge resource utilization, and proposed a fragmentation-aware bilevel VNE algorithm that enhances request acceptance and infrastructure profit. However, all these approaches are ultimately limited by the one-to-one node mapping constraint, which prevents the full integration of computing resources enabled by networking capabilities in CPN scenarios. Zhang et al. [19] relaxed this restriction by allowing multiple virtual nodes from the same virtual network to be co-located on a single substrate node, improving mapping efficiency. However, as a heuristic algorithm tailored for network emulation platforms, this work is not generally applicable to CPN environments and is still prone to local optima.

B. Service Function Co-location Technologies

SF Instantiation: Containerization has become a foundational technology in cloud-native environments due to its lightweight virtualization and efficient resource isolation capabilities. By encapsulating each service function within its own container, multiple SFs can be flexibly co-located on a single host, thereby improving resource utilization and deployment agility [5]. Such co-location is enabled by Linux namespaces and control groups (or cgroups) [21], which provide strong isolation between containers and allow for the independent management of resources, such as CPU and memory. In addition to CPU and memory resources, various technologies have emerged to enable efficient GPU sharing and management among containers [22].

SF Communication: At the node level, co-located SFs can flexibly establish arbitrary Layer 2 communication networks via technologies such as veth pairs and Open vSwitch (OVS), enabling intra-host data transmission and reducing inter-node network resource consumption [21]. At the domain level, SFs deployed in different data centers within a domain can establish communication links through tunneling technologies such as VxLAN, allowing traffic to remain within the domain and thus preserving valuable inter-domain network resources. Furthermore, per-flow traffic engineering (TE) tunnels enable logical links to be precisely mapped onto arbitrary forwarding paths in the CPN network, allowing for flexible and fine-grained network control [23].

Nevertheless, there remains a lack of theoretical guidance on how to exploit these new capabilities for service mapping in CPN. Therefore, it is imperative to develop new theoretical models and solution frameworks that can systematically leverage advanced co-location mechanisms to optimize service satisfaction and resource utilization.

III. Model Formulation and Problem Study

This section details the system model and mathematical formulation of the SEM problem. We then establish its theoretical intractability, analyze its practical challenges, and provide key insights for designing effective solutions.

A. System Model

1) Computing Power Network (CPN): The underlying CPN topology is formally defined as an undirected graph $G^s = (N^s, L^s)$ [12], where N^s represents the set of computing nodes (CNs) and L^s denotes the set of their interconnecting network links (NLs). In this paper, the superscript s corresponds to the CPN topology. Each CN $m^s \in N^s$ is characterized by its available computing capacity, denoted as $C(m^s)$. Similarly, each NL connecting a pair of CNs, $l^s_{mn} \in L^s$ $(\forall m^s, n^s \in N^s)$, with possessing a specific bandwidth capacity $B(l^s_{mn})$.

2) Service Entity (SE): Each service request i corresponds to an SE, modeled as an undirected graph $G^v_i = (N^v_i, L^v_i)$ [27]. In this representation, N^v_i represents the set of service functions (SFs), and L^v_i denote the set of logical links (LLs) connecting these SFs. For simplicity and without loss of generality, we primarily focus on CPU resources to define the computational requirements of SFs. Specifically, each SF $u^v \in N^v_i$ demands $c(u^v)$ units of CPU resources; each LL $l^v_{uw} \in L^v_i$, connecting a pair of SFs $u^v, w^v \in N^v_i$, is associated with a bandwidth requirement of $b(l^v_{uw})$.

B. Problem Description and Formulation

We address the SEM problem within an online system where service requests arrive sequentially and dynamically. The main challenge is to map each incoming SE, which temporarily consumes computing and network resources within

the CPN environment, by making real-time decisions based on instantaneous resource availability. We consider SEM as a sequential online optimization problem. Specifically, given a CPN topology $G^s = (N^s, L^s)$ and an incoming SE $G_i^v = (N_i^v, L_i^v)$, the SEM problem is abstracted into two sequential phases: the service function mapping (SFnM) and the logical link mapping (LLnM).

1) Service Function Mapping (SFnM): This phase maps each SF of G_i^v to an appropriate CN in G^s. A single CN can host multiple SFs (SF co-location), and each mapped SF consumes specified computing resources. We introduce a binary variable $x_{m^s}^{u^v} = \{0,1\}$ to indicates if SF $u^v \in N_i^v$ is mapped to a CN $m^s \in N^s$. The SFnM phase is subject to the following constraints:

• *SF-to-CN mapping:* Each SF must be mapped to exactly one CN (Equation (1)).

$$\forall u^v \in N_i^v : \quad \sum_{m^s \in N^s} x_{m^s}^{u^v} = 1 \tag{1}$$

• *CN-to-SF hosting:* A CN can host zero or more SFs (Inequality. (2)).

$$\forall m^s \in N^s : \quad \sum_{u^v \in N_i^v} x_{m^s}^{u^v} \geq 0 \tag{2}$$

• *CN resource capacity:* The total CPU requirements of hosted SFs must not exceed the CN's available capacity (Inequality (3)).

$$\forall m^s \in N^s : \quad \sum_{u^v \in N_i^v} x_{m^s}^{u^v} \cdot c(u^v) \leq C(m^s) \tag{3}$$

2) Logical Link Mapping (LLnM): This phase maps links of G_i^v to network paths (tunnels) within G^s [23]. For each pair of CNs $k = (m_s, n_s) \in K$, a set of loop-free paths P^k are pre-computed, where $P^s = \cup_{k \in K} P^k$. A binary variable $y_{m^s n^s}^p = \{0,1\}$ indicates if tunnel p uses the network link (NL) l_{mn}^s. If an LL's endpoint SFs are co-located on the same CN, its flow is routed internally; otherwise, it must be mapped to an external tunnel (referred to as a *Cut*-LL). We use binary variable $f_{p,k}^{u^v w^v} = \{0,1\}$ to indicate if LL l_{uw}^v is routed on tunnel $p \in P^k$. The LLnM phase is governed by the following constraints:

• *Flow indivisibility:* Each LL, if not internally hosted, must be mapped to at most one tunnel (Inequality (4)).

$$\forall l_{uw}^v \in L_i^v : \quad \sum_{k \in K} \sum_{p \in P^k} f_{p,k}^{u^v w^v} \leq 1 \tag{4}$$

• *Tunnel selection coherence:* A tunnel can only be selected for an LL if its endpoint SFs are mapped to the tunnel's respective CNs (Inequality (5)).

$$\begin{aligned} \forall l_{uw}^v \in L_i^v, \forall k = (m^s, n^s) \in K, \forall p \in P_k : \\ f_{p,k}^{u^v w^v} \leq x_{m^s}^{u^v} + x_{n^s}^{w^v} - 1, \\ f_{p,k}^{u^v w^v} \leq x_{n^s}^{u^v} + x_{m^s}^{w^v} - 1 \end{aligned} \tag{5}$$

• *Network Link (NL) resource capacity:* The total bandwidth requirements of mapped LLs must not exceed the capacity of any traversed NL (Inequality (6)).

$$\begin{aligned} \forall l_{mn}^s \in L^s : \\ \sum_{l_{uw}^v \in L_i^v} \sum_{k \in K} \sum_{p \in P^k} f_{p,k}^{u^v w^v} \cdot y_{m^s n^s}^p \cdot b(l_{uw}^v) \leq B(l_{mn}^s). \end{aligned} \tag{6}$$

Problem Formulation. Upon receiving a new service request, the CPN orchestrator solves the SEM problem to optimize SFnM and LLnM decisions, aiming to maximize *long-term system profitability*. This Profit metric balances service acceptance, revenue, and resource costs. The SEM problem is modeled as $\mathbb{P}1$:

$$\begin{aligned} (\mathbb{P}1) : \max_{\mathbf{x^t}, \mathbf{f^t}} \quad & \underbrace{(p_{ac}(t))^\theta}_{\substack{\text{Weighted} \\ \text{Acceptance Ratio}}} \cdot \underbrace{\left(\underbrace{\sum_{G_i^v \in \Upsilon^a(t)} \mathcal{R}(G_i^v)}_{\text{Revenue}} - \omega \cdot \underbrace{\sum_{G_i^v \in \Upsilon^a(t)} \mathcal{C}(G_i^v)}_{\text{Weighted Cost}} \right)}_{\text{Net Revenue (Profitability Core)}} \\ s.t. \quad & (1) - (6), \qquad \forall t. \end{aligned} \tag{7}$$

Here, $\mathbf{x^t}$ and $\mathbf{f^t}$ represent the SF and LL mapping decisions at time t. The objective (7) balances the weighted service acceptance ratio with net revenue. The coefficient $\theta \geq 1$ emphasizes the importance of the acceptance ratio, directly enhancing service satisfaction. The factor $0 < \omega < 1$ allows trading network resource consumption for higher computing resource utilization, aligning with CPN's goal of maximizing distributed computing resource use. The core components of the objective function are:

Acceptance ratio $p_{ac}(t)$: The proportion of successfully mapped SEs up to time t.

$$p_{ac}(t) = \frac{|\Upsilon^a(t)|}{|\Upsilon(t)|}, \tag{8}$$

where $\Upsilon(t)$ is the set of requested SEs and $\Upsilon^a(t)$ is the subset of successfully mapped ones.

Revenue $\mathcal{R}(G_i^v)$: Revenue from an accepted G_i^v, derived from its SF and LL resource demands. Rejected requests yield zero revenue.

$$\mathcal{R}(G_i^v) = \sum_{\forall u^v \in N_i^v} c(u^v) + \sum_{\forall l_{uw}^v \in L_i^v} b(l_{uw}^v). \tag{9}$$

Cost $\mathcal{C}(G_i^v)$: Resources consumed to host G_i^v comprising computing node cost $\mathcal{C}_n(G_i^v)$ and network link cost $\mathcal{C}_l(G_i^v)$.

$$\begin{aligned} \mathcal{C}(G_i^v) &= \mathcal{C}_n(G_i^v) + \mathcal{C}_l(G_i^v) \\ &= \sum_{\forall u^v \in N_i^v} c(u^v) + \sum_{\forall l_{uw}^v \in L_i^v} \sum_{k \in K} \sum_{p \in P^k} f_{p,k}^{u^v w^v} \cdot y_{m^s n^s}^p \cdot b(l_{uw}^v). \end{aligned} \tag{10}$$

Computing cost equals SF resource demands. Network cost varies based on the number of physical network links used for LL mapping.

C. Theoretical Analysis of SEM

No existing method can optimally solve online Integer Linear Programming (ILP) problems such as ($\mathbb{P}1$) in a time-efficient manner. Therefore, a widely adopted approach is to make independent optimization decisions for each service request based on current system states [28], [29]. In fact, even the offline version of this problem for a single request is NP-Hard, which makes exact optimization intractable. Without such simplification, it is extremely challenging to analyze or implement practical solutions in real-world settings. For this reason, we employ this local greedy strategy to simplify the original problem, albeit at the expense of compromising global optimality. Specifically, for a newly arrived request with arrival time τ, we transform the original problem ($\mathbb{P}1$) into an corresponding local optimization problem ($\mathbb{P}2$) specific to this request, which is illustrated as[1]:

$$(\mathbb{P}2): \max_{\mathbf{x},\mathbf{f}} (p_{ac}(\tau))^{\theta} \cdot \Big(\mathcal{R}(G_i^v) - \omega \cdot \mathcal{C}(G_i^v, \mathbf{x}, \mathbf{f})\Big) \tag{11a}$$

$$s.t. \quad (1)-(6). \tag{11b}$$

Because ($\mathbb{P}2$) is derived as a simplified offline version of ($\mathbb{P}1$) for individual requests, it eliminates some of the complexities associated with online decision-making and is therefore more tractable than ($\mathbb{P}1$).

At this time, with both the acceptance ratio and expected revenue being constant, maximizing the objective in ($\mathbb{P}2$) reduces to minimizing the bandwidth resource cost during LLnM:

$$(\mathbb{P}2-a): \min_{\mathbf{x},\mathbf{f}} \mathcal{C}_l(G_i^v, \mathbf{x}, \mathbf{f}) \qquad s.t. \quad (1)-(6). \tag{12}$$

We use ($\mathbb{P}2$-a) to represent a simplified but equivalent version of ($\mathbb{P}2$), which helps us prove the intractability of both ($\mathbb{P}2$) and the more challenging ($\mathbb{P}1$).

Statement 1 (($\mathbb{P}2$)'s decision version, ($\mathbb{P}2$)-D)**.** *Given the CPN topology $G^s = (N^s, L^s)$, the request's SE topology $G_i^v = (N_i^v, L_i^v)$ at timestamp τ, and a positive number Q, the problem is to ask whether there exists a mapping solution that keeps the LLnM cost (12a) no greater than Q while satisfying the constraints (12b).*

Statement 2 (Graph bisection problem (GBP)'s decision version, GBP-D)**.** *Given an undirected graph $G(V, E)$ and an integer K within the range $0 < K \leq |E|$, the problem involves determining whether V can be divided into two disjoint, equally sized vertex subsets V_1 and V_2 (i.e., $||V_1| - |V_2|| \leq 1$), such that their union spans all vertices ($V_1 \cup V_2 = V$) and their intersection is empty ($V_1 \cap V_2 = \emptyset$), while ensuring the number of edges connecting V_1 and V_2, denoted as $|Cut(V_1, V_2)|$, does not exceed K.*

Theorem 1. *($\mathbb{P}2$) is NP-Hard.*

Proof. To prove it, we reduce GBP-D to ($\mathbb{P}2$)-D. Let $\{G(V, E), V_1, V_2, K\}$ be an arbitrary instance of GBP-D. On this basis, we construct an instance of ($\mathbb{P}2$)-D with a CPN topology $G^s = (N^s, L^s)$, a request's SE topology $G_i^v = (N_i^v, L_i^v)$, and a threshold $Q > 0$. Then, we prove that a feasible ($\mathbb{P}2$)-D solution exists if and only if there exists a valid graph bisection for $\{G(V, E), V_1, V_2, K\}$ [30].

First, we design a polynomial-time transformation, in which we construct the SE topology $G_i^v = (N_i^v, L_i^v)$ and the CPN topology $G^s = (N^s, L^s)$ according to the given GBP-D instance. For the SE topology, let $N_i^v = V$ and $L_i^v = E$, with unit resource requirements for each SF and LL. The CPN topology comprises three CNs: $N^s = \{n_1, n_2, n_3\}$ and two LLs: $L^s = \{l^s_{n_1 n_2}, l^s_{n_2 n_3}\}$, with n_1 allocated $|V_1|$ resource units, n_2 containing $|V_2|$ resource units, and $|n_3|$ possessing no available resources, while all LLs maintain infinite bandwidth capacity. The threshold Q is set as $Q = 2K$. The above construction can be easily verified as polynomial-time computable.

We now establish the bi-directional reduction. If there exists a balanced bipartition (V_1, V_2) where $||V_1| - |V_2|| \leq 1$ and $|Cut(V_1, V_2)| \leq K$, then a feasible solution for ($\mathbb{P}2$)-D is constructed by the following mapping: map all SFs in V_1 to n_1, where $|V_1|$ equals the capacity of n_1; map all SFs in V_2 to n_2, where $|V_2|$ equals the capacity of n_2. Consequently, the LLs corresponding to $|Cut(V_1, V_2)|$ have to be carried through the NLs $l^s_{n_1 n_2}$ and $l^s_{n_2 n_3}$. The LLnM cost of the above solution is $\tilde{Q} = 2\tilde{K} \leq 2K = Q$.

Conversely, If there exists a feasible transformed solution to ($\mathbb{P}2$)-D with cost $\tilde{Q} \leq Q$, then since n_3 has zero capacity, all SFs must map to either n_1 or n_2. Let V_1 and V_2 be the sets of nodes mapped to n_1 and n_2, respectively. Here, the balanced condition $||V_1| - |V_2|| \leq 1$ is automatically satisfied by the capacity constraints of CNs. Moreover, since the LLnM process involves two NLs, $\tilde{K} = \tilde{Q}/2 \leq Q/2 = K$. Thus, a GBP-D problem can be reduced to a ($\mathbb{P}2$)-D problem.

Since the GBP-D problem is NP-Hard, the ($\mathbb{P}2$)-D problem is also NP-Hard. Note that ($\mathbb{P}2$)-D is the original ($\mathbb{P}2$)'s decision version, which is believed to be less intractable than the latter. Eventually, we prove that ($\mathbb{P}2$) is NP-Hard. ■

Corollary 1. *($\mathbb{P}1$) is NP-Hard.*

Proof. Since ($\mathbb{P}1$) is more intractable than ($\mathbb{P}2$), and ($\mathbb{P}2$) is NP-Hard by Theorem 1, ($\mathbb{P}1$) is NP-Hard. ■

D. Practical Challenges of SEM

While Theorem 1 establishes the NP-Hardness of ($\mathbb{P}1$), its practical resolution is further complicated by the new characteristics and associated challenges introduced by allowing SF co-location in the SEM problem. We illustrate these complexities with the following example.

Consider the scenario in Fig. 2, which involves two SEs representing incoming requests and examines how mapping decisions for the first request affect the feasibility of mapping the second. SFs are labeled with lowercase letters, with their CPU requirements shown inside each node. Each LL requires 1 unit of bandwidth. The CPN environment contains four CNs (labeled by capital letters), with node and link resource capacities indicated by the adjacent numbers.

Since co-located SFs jointly affect each CN's remaining resources and the total bandwidth requirement of LLs that

[1]Here, for convenience of expression, we use subscript i to denote the service request at timestamp τ

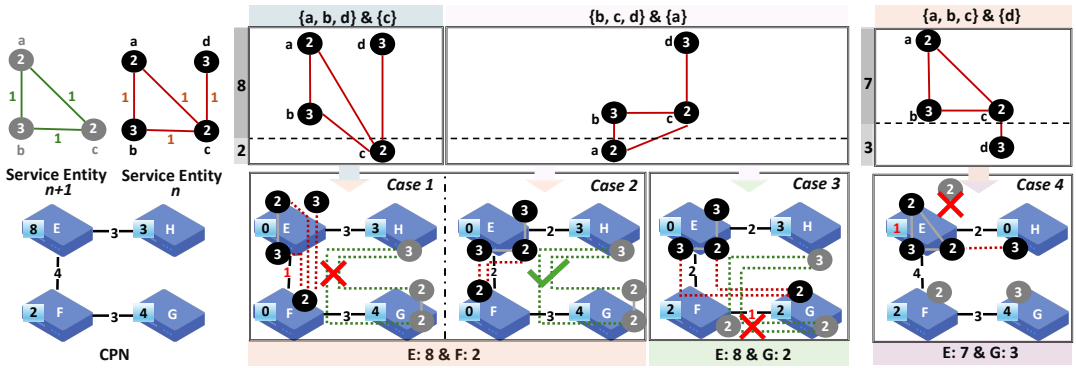


Fig. 2. Examples illustrating the additional complexities and challenges of the SEM problem introduced by SF co-location. The mapping solutions that lead to the rejection of the subsequent request are marked with red crosses, and the resource bottleneck locations causing the issue are indicated with red numbers.

must be mapped onto tunnels (*Cut*-LLs), node-level decisions alone cannot capture the global impact of mapping. To characterize the complexity and intertwined global effects of such decisions, we introduce three high-level observation perspectives that explicitly reflect the collective influence of co-located SFs, as shown in Fig. 2:

(a) Co-location group, which describes how SFs are grouped together based on their aggregate computational requirements within an SE (e.g., *8:2 and 7:3 in the example);*

(b) Co-location group assignment, which specifies the particular SF members for a given group (e.g., *{a,b,d}&{c} for 8:2 and {a,b,c}&{d} for 7:3); and*

(c) Co-location group mapping, which determines how each co-location group is mapped onto CNs (e.g., *E:8 & F:2 for 8:2 and E:7 & G:3 for 7:3).*

Co-location group, mapping, and assignment choices have different impacts on the computing and network resources of the CPN environment. The choice of co-location group (*e.g., 7:3 vs. 8:2*) affects computational utilization in CPN; for example, a 7:3 grouping inevitably leaves 1 unit of computing fragment at CN *E*, regardless of group assignment or mapping. For the same group assignment (*e.g., {b,c,d} & {a}*), different group mappings (*E:8 & F:2 vs. E:8 & G:2*) result in different NL usages; mapping to *G* instead of *F* adds *F–G* link usage, making it a bottleneck. With the same group mapping (*e.g., E:8 & F:2*), different group assignments (*{a,b,d} & {c} vs. {b,c,d} & {a}*) change the bandwidth requirements across all *Cut*-LLs; for instance, *{a,b,d} & {c}* increases the requirement from 2 to 3 and causes the *E–F* link to become a bottleneck. All these scenarios may block subsequent requests. These observations highlight the practical challenges in solving the SEM problem and offer valuable design insights.

Challenge 1: Strong coupling between SFnM variables induces complex cascading effects. Decision variables interact in a multidimensional and dynamic manner across computing and network resources, rendering node-level approaches inadequate.

Insight 1: Reformulate the problem via graph partitioning [31]. Treating each co-location group as a partitioning weight, assigning as partitioned subgraphs, and mapping as subgraph placement on CNs, better captures these couplings and allows joint optimization (§ IV-A).

Challenge 2: The combinatorial solution space grows explosively, making global optimality harder to achieve and local search heuristics prone to local optima; when $|N^v| \leq |N^s|$, the number of SFnM combinations increases from $A^{|N^v|}_{|N^s|}$ to $|N^v|^{|N^s|}$.

Insight 2: Enable adaptive search via explicit coupling. Guided by global metrics and by prioritizing assignments that minimize *Cut*-LL bandwidth, jointly searching over groupings and mappings avoids premature convergence and effectively explores the solution space. (§ IV-B).

Challenge 3: The enlarged solution space and strong coupling hinder effective global evaluation; local metrics [28] often lead to suboptimal results (e.g., Case 4 minimizes bandwidth cost of *Cut*-LL mapping but is not globally optimal).

Insight 3: Assess global impact using resource fragmentation. Resource fragmentation, especially from bottlenecks (Cases 1, 3, 4), serves as a proxy for the global effect of decisions. Quantifying fragmentation guides the search for better global solutions (§ IV-C).

IV. ABS: Framework Design and Implementation

Based on the identified insights, this section reformulates the problem, designs the search framework, and develops a global evaluation mechanism.

A. Reformulation for Coupling-Aware Decision-Making

In addition to the coupling among SFnM variables, a major challenge in SEM arises from the deep interdependence between SFnM and LLnM. As shown in Fig. 2, co-location group decisions shape the bandwidth needs and tunnel options for *Cut*-LLs, directly affecting LLnM bandwidth costs as in (10). Conversely, suboptimal *Cut*-LL mappings in LLnM can fragment CN resources: network resource depletion or uneven allocation may leave computing resources scattered across nodes, without enough network resources to interconnect and aggregate them for future SFnM. This tight coupling complicates joint optimization across both processes.

Therefore, we adopt a local greedy approach based on the ($\mathbb{P}$2-a) problem, decomposing SEM into a more tractable two-phase structure. In phase one, we solve the minimum-cut SF mapping (mcuSm) for SFnM, identifying co-location

groups, assignments, and mappings that minimize the bandwidth requirements of *Cut*-LLs. In phase two, we solve the minimum-cost LL mapping (mcoLm) for LLnM, using the SFnM solution to minimize the additional bandwidth costs from mapping these *Cut*-LLs. While this dual-phase method cannot guarantee global optimality due to the coupling between SFnM and LLnM, it provides a practical approach to decouple the problem and focus on the complex interactions among SFnM decision variables.

1) The mcuSm optimization: This optimization problem is formulated as:

$$\mathbb{P}3: \min_{\mathbf{x}} \sum_{\forall l_{uw}^v \in L_i^v} b(l_{uw}^v) \sum_{\forall m^s \in N^s} x_{m^s}^{u^v}(1 - x_{m^s}^{w^v}) \tag{13a}$$

$$s.t. \quad (1) - (3). \tag{13b}$$

Corollary 3 proves the intractability of ($\mathbb{P}3$); however, this formulation provides a foundation to systematically achieve coupling-aware decision making. According to ***Insight 1***, we first introduce a unique form of graph partitioning [31] to formulate an equivalent problem to ($\mathbb{P}3$), thereby transforming the SFnM process from independent decision-making into a coupling-aware joint decision-making form.

Definition 1 (Proportional Weight-Constrained k-way Graph Partitioning Problem, PW-kGPP)**.** *Consider an undirected graph $G = (V, E)$, where each vertex $i \in V$ has a vertex weight $w_i > 0$, each edge $(i, j) \in E$ has an edge weight $c_{ij} > 0$, and a normalized weight proportion set $PS = \{r_1, r_2, ..., r_k\}$ satisfies $\sum_{p=1}^{k} r_p = 1$. The problem requires partitioning V into k disjoint subsets $V_1, V_2, ..., V_k$, such that the sizes of the subsets correspond to the given proportion weights, while minimizing the total weight of the cut edges (edges connecting different subsets). The formal formulation is provided in Appendix A.*

According to Definition 1, we reformulate the ($\mathbb{P}3$) problem and propose the problem ($\mathbb{P}4$):

$$\mathbb{P}4: \min_{\boldsymbol{\rho},\mathbf{x}} \sum_{\forall l_{uw}^v \in L_i^v} b(l_{uw}^v) \sum_{\forall m^s \in N^s} x_{m^s}^{u^v}(1 - x_{m^s}^{w^v}) \tag{14a}$$

$$s.t. \quad (1) - (3), \tag{14b}$$

$$\forall m^s \in N^s:$$

$$(1-\theta)\rho_{m^s} \le \frac{\sum_{u^v \in N_i^v} c(u^v) x_{m^s}^{u^v}}{\sum_{u^v \in N_i^v} c(u^v)} \le (1+\theta)\rho_{m^s}, \tag{14c}$$

$$\forall u^v \in N_i^v, \forall m^s \in N^s: \quad x_{m^s}^{u^v} \le \frac{\rho_{m^s}}{\epsilon}, \tag{14d}$$

$$\sum_{m^s \in N^s} \rho_{m^s} = 1, \tag{14e}$$

where ϵ is a minimal positive number (e.g., $\epsilon = 10^{-6}$), used to ensure that when $\rho_{m^s} = 0$, $x_{m^s}^{u^v}$ is imposed to be 0.

The optimization object of ($\mathbb{P}4$) is the same as that of ($\mathbb{P}3$), whose binary decision variable $x_{m^s}^{u^v}$ characterize the standard SFnM process. Note that we define a new continuous decision variable, ρ_{m^s}, representing the ratio of the total resource requirements of all SFs mapped to CN m^s to the total resource requirement of all SFs in the current service request. A "subpart" of a SE is defined here as the combination of SFs and the LLs between them that are assigned together to a single CN.

Similar to (28b), (14c) constrains which SFs can be grouped on CN m^s to form a subpart, while also limiting the tolerance between the actual proportion of resources mapped to each m^s and the specified ρ_{m^s}. (14d) ensures that all SFs are mapped to CNs, with the corresponding proportions constrained to be greater than 0. The sum of the proportions corresponding to all CNs must equal 1, ensuring that all SFs can be fully mapped, as described by (14e).

According to the definitions, and as illustrated in the examples in Fig. 2, it can be observed that under the given constraints, the variable ρ_{m^s} jointly determines the co-location group and its mapping, while the variable $x_{m^s}^{u^v}$ determines the assignment of the co-location group. In other words, ($\mathbb{P}4$) provides a structured formulation that better captures the intricate couplings between SFnM variables and enables joint optimization, as motivated by our ***Insight 1***. In the following, we prove the equivalence between ($\mathbb{P}3$) and ($\mathbb{P}4$).

Theorem 2. *($\mathbb{P}3$) and ($\mathbb{P}4$) are equivalent.*

Proof. The formal proof appears in Appendix A. ■

Unfortunately, both ($\mathbb{P}3$) and ($\mathbb{P}4$) are still NP-Hard problems. However, we observe that if a set of feasible proportions $\boldsymbol{\rho}$ is given, ($\mathbb{P}4$) reduces to the PW-kGPP problem. In this reduction, non-zero values of ρ in ($\mathbb{P}4$) correspond to the weight proportion set PS in PW-kGPP, with the number of non-zero elements equal to k, and other correspondences following directly. Although PW-kGPP is also NP-Hard, various heuristic and practical algorithms are available to efficiently obtain near-optimal solutions [31].

Theorem 3. *The PW-kGPP problem is NP-Hard.*

Proof. See Appendix A for details. ■

Corollary 2. *($\mathbb{P}4$) is NP-Hard.*

Proof. See Appendix A for details. ■

Corollary 3. *($\mathbb{P}3$) is NP-Hard.*

Proof. See Appendix A for details. ■

2) The mcoLm optimization: After the mcuSm optimization, the set of *Cut*-LLs, denoted as CL_i^v, is determined. The next step is to map each $l_{uw}^v \in CL_i^v$ onto a tunnel, with the objective of minimizing the total bandwidth cost. This mapping subproblem can be reduced to an instance of the Integer Multicommodity Flow Problem (IMCF), which is well known to be NP-Hard [32].

B. Bilevel optimization framework for adaptive searching

Inspired by ***Insight 2***, we reformulate ($\mathbb{P}4$) as an equivalent bilevel optimization problem (BOP), as shown below, to leverage its advantages: enabling adaptive search guided by global evaluation metrics at the upper level, while ensuring local optimality at the lower level during practical solution

procedures, thereby allowing more efficient search in large solution spaces [33].

$$(\mathbb{P}4-BOP):\tag{15a}$$

$$\text{Upper-level}\min_{\boldsymbol{\rho}}\sum_{\forall l^v_{uw}\in L^v_i} b(l^v_{uw})\sum_{\forall m^s\in N^s} x^{u^v}_{m^s}(1-x^{w^v}_{m^s})$$

$$s.t.(14c)\tag{15b}$$

$$\text{Lower-level}\min_{\mathbf{x}} 0\quad(\text{A fictitious objective})\tag{15c}$$

$$s.t.(14c),(14d),(14e)\tag{15d}$$

Lemma 1. *The optimal solutions to ($\mathbb{P}4$) are feasible solutions to ($\mathbb{P}4-BOP$).*

Proof. Details are provided in Appendix A. ■

Lemma 2. *The optimal solutions to ($\mathbb{P}4-BOP$) are feasible solutions to ($\mathbb{P}4$).*

Proof. Please refer to Appendix A. ■

Theorem 4. *($\mathbb{P}4-BOP$) and ($\mathbb{P}4$) are equivalent.*

Proof. See Appendix A for details. ■

Taking a closer look, the aforementioned dual-phase structure enables us to first solve the mcuSm optimization, then, based on its result, solve the mcoLm optimization (i.e., the IMCF problem). Furthermore, the bilevel nature of mcuSm leads to a two-stage process: we first search for the upper-level variable set $\boldsymbol{\rho}$; given any fixed $\boldsymbol{\rho}$, the lower-level subproblem reduces to a PW-kGPP problem. Through this series of decomposition and reformulation, we obtain a practical search framework for ($\mathbb{P}2$)—search over possible $\boldsymbol{\rho}$ at the upper level, and for each candidate $\boldsymbol{\rho}$, solve the corresponding PW-kGPP and IMCF subproblems to obtain a feasible solution $(\mathbf{x},\mathbf{f})$. Accordingly, we state the following proposition.

Proposition 1. *Suppose the outer layer can traverse all possible values of $\boldsymbol{\rho}$, and the inner layer will accurately solve the corresponding problems. The final solution obtained by the nested approach will be the optimal one for ($\mathbb{P}2$).*

Proof. Details are provided in Appendix A. ■

According to Proposition 1, even though the PW-kGPP and IMCF problems are intractable and only suboptimal solutions are attainable in practice, the proposed search framework can still converge to near-optimal solutions for ($\mathbb{P}2$). Notably, efficient algorithms exist for these subproblems under certain conditions: the balanced graph partitioning problem (a special case of PW-kGPP) admits an $O(\log n)$ approximation [34], and heuristics such as METIS [31] perform well empirically for general PW-kGPP. For IMCF, the k-shortest path algorithm provides high-quality candidate paths for each *Cut*-LL.

In summary, by systematically exploring the feasible region of the proportion weight vector (PWV), $\boldsymbol{\rho}$, and leveraging state-of-the-art practical algorithms for the PW-kGPP and IMCF subproblems, a suboptimal solution to ($\mathbb{P}2$) can be obtained. However, since this approach addresses each request individually using a local greedy strategy, it remains inherently myopic. To overcome this limitation and guide the search toward high-quality solutions for the original global objective of ($\mathbb{P}1$), it is crucial to incorporate global evaluation metrics that account for cumulative performance across the entire online process.

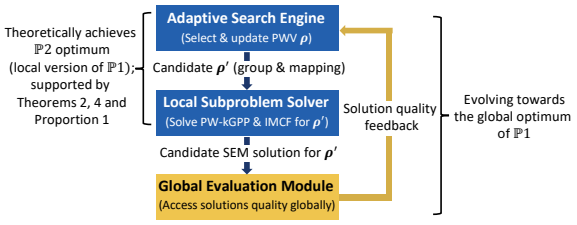


Fig. 3. Architecture of the Adaptive Bilevel Search (ABS) framework for the SEM problem.

Motivated by the above theoretical framework, we propose the ABS framework (Fig. 3). As a modular architecture, ABS integrates global strategic guidance with local optimization for SEM problems. It consists of three interdependent core components that form an iterative feedback loop, enabling dynamic adjustments and systematic convergence toward the global optimum:

- Adaptive Search Engine: It employs adaptive strategies to traverse the PWV space in search of an optimal $\boldsymbol{\rho}$. Based on feedback from the Global Evaluation Module, it prioritizes regions with high SEM solution quality and dynamically refines its search trajectory.
- Local Subproblem Solver: It efficiently solves the PW-kGPP and IMCF subproblems using state-of-the-art algorithms to produce the corresponding solution, which the Dynamic Evaluation Module then evaluates.
- Global Evaluation Module: It assesses the SEM solution quality from a global perspective and provides real-time feedback to the Adaptive Search Engine, guiding its exploration of the PWV space toward promising regions.

By employing a feedback strategy to iteratively refine $\boldsymbol{\rho}$ toward the global optimum and ensuring local optimality of each subproblem, ABS effectively bridges the gap between global (online) and local (offline) optimization.

C. Fragmentation-Based Metrics for Global Evaluation

According to ***Insight 3***, it is necessary to evaluate each mapping decision found by ABS in real time based on the current fragmentation state, thereby further enhancing its iterative capability toward the global optimum. To overcome the limitations of conventional load-dependent and resource-centric fragmentation evaluation methods [22], we propose a service-centric approach that focuses on the immediate impact of each mapping decision on resource utilization, without relying on any prior knowledge of input service entities.

We first provide additional definitions for the evaluated mapping decision $(\hat{\mathbf{x}},\hat{\mathbf{f}})$ to facilitate expression. Let N^s_i denote the set of all CNs participating in hosting SFs in the decision $(\hat{\mathbf{x}},\hat{\mathbf{f}})$[2]. Then, the resource amount utilized of any participating CN, $m^s\in N^s_i$, can be formulated as:

$$P_C(m^s)=\sum_{u^v\in N^v_i}\hat{x}^{u^v}_{m^s}\cdot c(u^v).\tag{16}$$

[2]The mapping decision in planning is defined as the one for the i^{th} request.

Besides, we denote each participating CN's correlated bandwidth consumption as:

$$P_{BW}(m^s) = \sum_{l_{uw}^v \in \hat{CL}_i^v} (\hat{x}_{m^s}^{u^v} + \hat{x}_{m^s}^{w^v}) \cdot b(l_{uw}^v). \quad (17)$$

Observing each of the three fragmentation scenarios exemplified in Fig. 2, we propose tailored evaluation metrics designed to prevent the formation of such fragments, where a higher metric value indicates a more desirable solution.

Node Resource Exhaustion Degree (NRED) quantifies the overall resource exhaustion level across all participating CNs. Inspired by Case 4, we establish a "using it all" criterion for each decision. Once a CN is selected to host SFs, SFs are mapped to consume as much of its available resources as possible, prioritizing their total resource requirements over their mere count. This approach minimizes residual computing resources on utilized nodes, thereby reducing potential resource fragmentation. It can be formulated as follows:

$$NRED = \frac{\sum_{m^s \in N_i^s} \left(\frac{P_C(m^s)}{C(m^s)} \right)}{\sum_{m^s \in N_i^s} \left[\max\left(1 - \frac{P_C(m^s)}{C(m^s)} - \delta,\, 0\right) \right] + \epsilon}, \quad (18)$$

where δ is a threshold parameter, and ϵ is a small constant preventing zero division. The numerator sums the resource utilization ratio, $\frac{P_C(m^s)}{C(m^s)}$, of each participating CN to reward node exhaustion, increasing as each node approaches full utilization. Meanwhile, the denominator equally penalizes the CNs that have not fully utilized their resources, where $1 - \frac{P_C(m^s)}{C(m^s)} > 0$, assigning a uniform penalty factor. The NRED value decreases as the number of under-utilized CNs increases. Moreover, the threshold δ excludes those nearly exhausted CNs (remaining ratio: $1 - \frac{P_C(m^s)}{C(m^s)} \leq \delta$) from penalties to enhance practical applicability. The optimal NRED value is achieved when all participating CNs are fully exhausted, leading to a denominator of ϵ and maximizing NRED.

Computing to Bandwidth Utilization Gap (CBUG) evaluates the overall computing-to-bandwidth utilization status of all participating CNs. In Case 1, CN *E* does not have sufficient bandwidth to support the LLs *b-a* and *b-c* in the next request. To avoid this situation, we expect that after each mapping, the remaining computing resources of a node are minimized, while its residual correlated bandwidth is maximized, thereby allowing the node to continue functioning as a forwarding node. Here, a CN's correlated bandwidth refers to the total available bandwidth of all NLs connected to it. We propose a "keeping the gap" bandwidth utilization strategy to achieve this purpose. In this design, the correlated bandwidth consumption should be as small as possible relative to the computing resource utilization for each participating CN m^s. That is, the ratio $\frac{P_C(m^s)}{P_{BW}(m^s)}$, which we refer to as the utilization gap, should be maximized. Furthermore, a larger gap indicates that more computing resources are utilized per unit of bandwidth consumed, thereby avoiding cases where bandwidth is exhausted while computing resources remain underutilized. **CBUG** is formulated as follows:

$$CBUG = \frac{\sum_{m^s \in N_i^s} \frac{P_C(m^s)}{P_{BW}(m^s)+\epsilon}}{|N_i^s|}, \quad (19)$$

where we set ϵ as a small constant to prevent zero division.

Path Node Valuelessness Level (PNVL) quantifies the impact of mapping *Cut*-LLs on computing resource utilization. During LLnM, a CN consumes bandwidth both for locally hosted SFs' *Cut*-LLs and, as a forwarding node, for tunnel paths. After SFnM, the residual computing resources of each CN are known; nodes with more resources are more valuable for future requests and should ideally be less involved in forwarding. For example, in Case 3 of Fig. 2, although CN *F* retains sufficient computing resources to host a future SF, it lacks the necessary bandwidth for associated LLs due to prior forwarding tasks. Therefore, we adopt a "traversing less valuable nodes" criterion and define a metric to evaluate the valuelessness level of forwarding nodes along the mapping path of each *Cut*-LL. Specifically, for a *Cut*-LL l_{uw}^v, $\hat{MoP}(l_{uw}^v)$ denotes the set of CNs acting as its forwarding nodes under decision $(\hat{\mathbf{x}}, \hat{\mathbf{f}})$, and the metric is formulated as:

$$P_{PV}(l_{uw}^v) = \frac{\sum_{m^s \in MoP(l_{uw}^v)} \frac{b(l_{uw}^v)}{C(m^s)-P_C(m^s)+\epsilon}}{e^{-|\hat{MoP}(l_{uw}^v)|}}, \quad (20)$$

where ϵ is a small constant to prevent zero division. In the numerator, we sum the ratios of each *Cut*-LL's bandwidth requirement to the residual computing resources of each forwarding node, discouraging the traversal of more valuable CNs. The denominator uses an exponential function to penalize paths with excessive hop counts, thereby limiting the number of forwarding nodes and reducing bandwidth consumption during LLnM. Based on this, we define **PNVL** to assess the overall impact of all *Cut*-LLs in a decision:

$$PNVL = \frac{\sum_{l_{uw}^v \in \hat{CL}i^v} PPV(l_{uw}^v) + \epsilon'}{|\hat{CL}_i^v| + \epsilon}, \quad (21)$$

where $\epsilon \ll \epsilon'$ prevent division by zero. This metric is the arithmetic mean of the path evaluation metrics across all *Cut*-LLs.

D. Implementation Details

We now present the ABS implementation via Distributed Particle Swarm Optimization, including the workflow, evolution, and initialization strategies, as well as a computational complexity analysis (see the pseudocode of Algorithms 1–4 in Appendix C).

1) Basic Idea: To implement the ABS framework, we adopt the distributed elite-guided learning particle swarm optimizer (DEGLSO) framework [35], which offers inherent scalability and flexibility for complex CPN scenarios. It builds on the classic Particle Swarm Optimization (PSO) algorithm by incorporating elite-guided learning and distributed computing strategies, enhancing both convergence speed and scalability.

From the perspective of ABS's architecture, we adopt the DEGLSO as the Adaptive Search Engine. We integrate our proposed fragmentation-based evaluation mechanism into

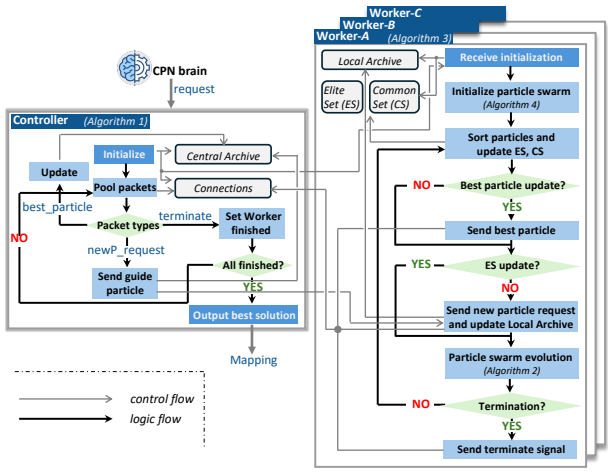


Fig. 4. ABS framework implementation scheme.

constructing the fitness function of PSO, serving as the Global Evaluation Module, which is formulated as:

$$\mathcal{F} = \frac{1}{\omega_1 \cdot NRED + \omega_2 \cdot CBUG + \omega_3 \cdot PNVL}, \tag{22}$$

where ω_1, ω_2, and ω_3 represent the weighting coefficients among the evaluation metrics. The specific values of these weights can be determined based on the observed correlation between higher values of these metrics and improved overall performance, as discussed in § V-B3. To solve the two subproblems, PW-kGPP and IMCF, we utilize METIS[3] and k-shortest path[4] as the Local Subproblem Solver.

However, DEGLSO was initially designed for general optimization problems, and its mechanisms do not fully align with the specific requirements of the ABS framework. The following subsections detail how we adapt and apply DEGLSO in our implementation.

2) Overall Workflow: Our ABS inherits the controller-worker model of DEGLSO, where the main procedure functions as the controller. During optimization, the controller aggregates and updates the global search state based on feedback from all the workers. Each worker independently manages a local particle swarm, performing iterative evolution updates under the guidance of the controller. After all workers complete their iterations, the controller selects the particle with the best fitness value among all reported results and uses its corresponding solution as the mapping decision for the current service request. If the workers cannot report any particles, this request will be rejected (see Fig. 4 for an overview).

Unlike general PSO approaches, where a particle's position directly represents a candidate solution, our implementation assigns the position a dual role. First, it explicitly encodes $\boldsymbol{\rho}$, the core variable updated during the search (referred to as the explicit position, or simply the position). Second, since fitness evaluation requires the SEM solution $(\mathbf{x}, \mathbf{f})$, this solution is derived from the explicit position $\boldsymbol{\rho}$ and forms the particle's implicit position (hereafter, the solution). Positions are updated via (23) and (24), while fitness is computed on the solution using $\mathcal{F}(\cdot)$ in (22).

[3]https://github.com/KarypisLab/METIS
[4]https://networkx.org/algorithms/shortest_paths.html

The controller maintains an archive as the core of the collaborative process, storing the current optimal particles reported by workers. This archive continuously incorporates the latest global search results and provides guidance for workers' evolutionary updates. Controller–worker collaboration is achieved through asynchronous communication: the controller establishes dedicated channels with each worker, monitors incoming messages, updates the archive, and responds with evolutionary guidance as needed. Once all workers have completed their iterations, the controller finalizes and returns the results. During the optimization process, communication occurs when a worker discovers a better local solution, requires guidance for further search, or finishes its computation. In each case, the controller evaluates new information, updates the archive if appropriate, and provides selected particles from the archive to guide the workers' evolution (see details in Fig. 4 and Algorithm 1).

3) Evolution Iteration Phase: During this phase, each worker in ABS maintains a local particle swarm and executes its evolutionary updates, driving the whole iteration process (see Fig. 4 for an overview).

To enhance high-dimensional search efficiency, we incorporate the elite-guided learning strategy of DEGLSO. In each iteration, the local swarm is divided into an elite set ($\mathbf{ES}$) and a common set ($\mathbf{CS}$) based on solution quality. Only particles in $\mathbf{CS}$ are updated, guided by both local elite particles (from the local archive, $\mathbf{LA}$) and historical best particles identified by different workers. This approach helps maintain diversity and enables particles to escape local optima.

Taking any dimension $d \in \{1, 2, ..., |N^s|\}$ of the vector $\boldsymbol{\rho}$ as an example, the update rule for the vectors of these common particles can be expressed as:

$$v_d^{t+1} = \underbrace{r_1 v_d^t}_{\text{inertia}} + \underbrace{r_2(e_d^t - \rho_d^t)}_{\text{a random elite}} + \underbrace{\phi r_3(\hat{E}_d^t - \rho_d^t)}_{\text{elites' mean position}}, \tag{23}$$

$$\rho_d^{t+1} = \rho_d^t + v_d^{t+1}, \tag{24}$$

$$\hat{E}^t = \frac{1}{|ES^t \cup LA^t|} \cdot \sum_{\rho \in ES^t \cup LA^t} \rho\,, \tag{25}$$

where $\boldsymbol{\rho}^t$ and $\mathbf{v}^t$ are the position and velocity of any particle in the $\mathbf{CS}^t$, respectively; $\boldsymbol{e}^t$ is the position of a randomly selected particle from $\mathbf{ES}^t \cup \mathbf{LA}^t$; $\hat{\mathbf{E}}^t$ is the means position of all the local elite particles; and t is the current iteration's index. Moreover, ϕ is a linear adjuster to enhance the exploitation at the late stages [36], expressed as:

$$\phi^t = 1 - \frac{t}{G_{max}}, \tag{26}$$

where t is the index of the current iteration, and G_{max} is the maximal iteration number. In our setting, high-dimensional sparsity emerges due to SF co-location, especially as the number of CNs increases, resulting in most PWV elements being zero. Such sparsity significantly complicates efficient search and reduces the likelihood of finding feasible solutions. To address this challenge, we introduce a separate search

mechanism. Specifically, each particle first performs unconstrained exploration in continuous space ($\boldsymbol{\rho}$), fully leveraging the flexibility of free search without imposing sparsity or normalization constraints. Subsequently, a dynamic top-n masking is applied, where only the n largest components of $\boldsymbol{\rho}$ are retained and normalized, yielding a sparse vector ($\boldsymbol{\rho}'$) that satisfies the simplex constraint. This sparse vector is then used as the PWV for solving the subproblems. If both subproblems yield feasible solutions, the result is assigned to the particle solution, and the search dimension n is reduced to progressively focus the search on the most critical variables (see details in Algorithm 2).

To support global optimization, each worker maintains its local state and collaborates with the controller. After initialization, the worker updates the **CS** of particles in each iteration. If the local best particle improves, this information is communicated to the controller. When no improvement occurs in the **ES**, the worker requests guidance and updates its **LA** based on feedback from the controller. The worker then proceeds to evolve the particles in the **CS** for the next iteration (see Fig. 4 and Algorithm 3 for details).

4) Initializaion Phase: Particle initialization must satisfy SEM structural constraints and sufficiently cover the solution space; otherwise, insufficient constraints may produce infeasible solutions and lead to many wasted iterations, while overly strict constraints can hinder exploration. To achieve this, we propose a semi-constrained randomized breadth-first initialization method, which efficiently initializes the particle swarm for each worker and supports effective iterations. For each particle, candidate CNs with abundant resources are probabilistically selected and expanded in a breadth-first manner to minimize inter-node distances, thereby reducing LLnM cost and improving SFnM feasibility. To ensure sufficient exploration, the process dynamically expands the candidate region, allowing broader network areas to be considered until a feasible solution is found or resources are exhausted. See Algorithm 4 for detailed steps.

5) Time Complexity Analysis: The overall computational complexity of the proposed distributed ABS implementation is primarily determined by the iterative main loop executed by each worker. It has polynomial time complexity, given by $\mathcal{O}(ITR_{max} \cdot |N_S| \cdot k \cdot |N^s| \cdot (|L^s| + |N^s| \log |N^s|))$, indicating that the algorithm can efficiently scale to large and complex problems through multi-worker parallelization. A detailed complexity analysis is provided in the Appendix C.

V. Performance Evaluation

A. Experimental Setup

1) Benchmarks: We compare our ABS against six algorithms spanning three mainstream categories: heuristic (**RW-BFS** [37], **RMD** [19]), meta-heuristic (**EA-PSO** [38], **GA-STP** [29]), and learning-based (**RL-QoS** [14], **GAL** [25]) methods. Note that all these algorithms are designed for the traditional VNE problem. For a fair comparison, we adapt them for the SEM problem by removing the one-to-one mapping constraint between SFs and CNs. Details of baselines are given in Appendix D.

TABLE I
Simulation Parameters

Parameters	CPN Topology		SE Topology
	Random	Rocketfuel	
Number of Topology	1	1	2000
Number of Nodes	100	129	50-100
Number of Links	500	363	*Random* (0.9)
Node CPU	400-600	400-600	1-20
Bandwidth	400-600	400-600	1-20
Arrival Time	-	-	*Poisson* (0.1)
Life Time	-	-	*Exp* (500)

2) Performance Metrics: For evaluating algorithm efficacy, our primary objectives are to maximize **acceptance ratio**, **revenue**, **long-term average revenue (LT-AR)**, **profit**, and **CN Resource Utilization (CU-Ratio)**. **Revenue to cost ratio (RC-Ratio)** and **long-term revenue to cost ratio (LT-RC-Ratio)** are also reported to provide a reference for cost efficiency, though we note their limitations as comprehensive evaluation metrics. Cost alone is not used as a primary metric, as, by definition, it not only reflects resource expenditure but may also indicate higher service acceptance and revenue. The metric details are also elaborated in Appendix D.

3) Simulator settings: We conduct simulations in a numerically generated environment to evaluate algorithm performance with online service requests. SE topologies arrive sequentially to a CPN topology, which is either a random Waxman model [37] or a real-world Rocketfuel (AS6461) instance [39]. To emulate complex services and dense inter-function dependencies, SEs are large-scale with high link connectivity [28]. Node and link resources are uniformly distributed. Request arrivals follow a Poisson process, and their lifetimes follow an exponential distribution. All specific simulation parameters are detailed in Tab. I.

The simulation experiments are conducted on a server equipped with an Intel(R) Xeon(R) Gold 5218R CPU @ 2.10GHz, an NVIDIA GeForce RTX 3080 GPU, and 252GB of RAM. The computational environment is based on Python 3.10.16, employing PyTorch 1.12.1 and PyTorch Geometric 2.2.0 as its machine learning frameworks. GPU acceleration is facilitated by driver version 515.65.01 and CUDA 11.7.

B. Performance Results and Analysis

1) Overall Performance: Tab. II presents the aggregated results of all algorithms over 2000 trials for all metrics (except for the CU-Ratio) under both CPN topologies. Note that $\text{APSDPS}_{\text{init by RW-BFS}}$ is a variant of ABS, where the `init_solver` function in the particle swarm initialization is replaced with the RW-BFS algorithm.

As shown in Tab. II and Fig. 6, ABS and its variant consistently achieve the best performance among all evaluated algorithms on the key metrics under both random and real-world topologies. This strong performance stems from several key design choices of ours. First, by adopting a graph partitioning perspective, ABS transforms independent mapping decisions into a co-location-aware search process, enabling effective SF grouping and mapping tailored for CPN scenarios.

TABLE II
COMPREHENSIVE EVALUATION OF ALL COMPARED ALGORITHMS. THE TOP THREE PERFORMANCES ARE HIGHLIGHTED USING **FIRST**, **SECOND**, AND **THIRD**.

	Algorithm	Acpt. Ratio ↑	Revenue ↑	LT-AR ↑	Profit ↑	RC-Ratio	LT-RC-Ratio
Testing Under Random Topology							
Heuristic	**RW-BFS** [37]	0.589	7720887	181175	1082950	0.839	0.841
	RMD [19]	0.381	4258676	100049	244752	0.827	0.828
Meta-Heuristic	**EA-PSO** [38]	0.523	6691894	154194	103220	0.530	0.531
	GA-STP [29]	0.416	4475305	105223	351589	0.916	0.931
Learning-Based	**RL-QoS** [14]	0.592	7676094	182007	571727	0.752	0.636
	GAL [25]	**0.613**	**8249720**	**190394**	**1305402**	0.865	0.871
Our Approach	**ABS**$_{\text{init by RW-BFS}}$	**0.693**	**9411934**	**218374**	**1487462**	0.745	0.753
	ABS	**0.703**	**9735826**	**228028**	**1613916**	0.752	0.751
Testing Under Real-World Topology							
Heuristic	**RW-BFS** [37]	0.234	2343136	57227	64054	0.999	0.997
	RMD [19]	0.036	350989	8333	242	1.072	1.046
Meta-Heuristic	**EA-PSO** [38]	0.135	1330372	32558	-675	0.487	0.502
	GA-STP [29]	0.22	2028733	47645	57195	1.198	1.205
Learning-Based	**RL-QoS** [14]	-	-	-	-	-	-
	GAL [25]	**0.256**	**2578649**	**60050**	**91009**	1.083	1.102
Our Approach	**ABS**$_{\text{init by RW-BFS}}$	**0.376**	**3927901**	**97433**	**246508**	0.899	0.878
	ABS	**0.410**	**4486683**	**103144**	**333456**	0.898	0.912

Moreover, its bilevel optimization structure efficiently explores the solution space via locally optimal subproblems. Finally, the resource fragmentation-based feedback mechanism offers a global evaluation metric that dynamically guides the search toward global optimality.

Among learning-based methods, GAL stands out among all baselines due to its two-stage design: it first imitates the node ranking pattern of RW-BFS using a graph neural network, and then refines its policy through reinforcement learning. It's worth noting that RL-QoS, although ranking fourth on the random topology, fails to converge effectively on the more network resource-constrained real-world topology. The main issue lies in RL-QoS's use of auto-regressive RL trained from scratch, which is prone to error accumulation and struggles with sparse rewards in challenging settings. In contrast, GAL's initial imitation learning phase enables more effective early exploration, which helps overcome these challenges.

RW-BFS maintains solid performance among heuristics by using topology-aware node ranking, often grouping nodes with similar scores and thus tending to co-locate SFs with comparable roles in the network. In contrast, RMD leverages graph partitioning to minimize the bandwidth requirement of *Cut*-LLs, ensuring co-location assignments are always optimal from the partitioning perspective. However, its reliance on rigid local greedy strategies often leads to suboptimal co-location groups and mappings, ultimately resulting in the poorest overall performance.

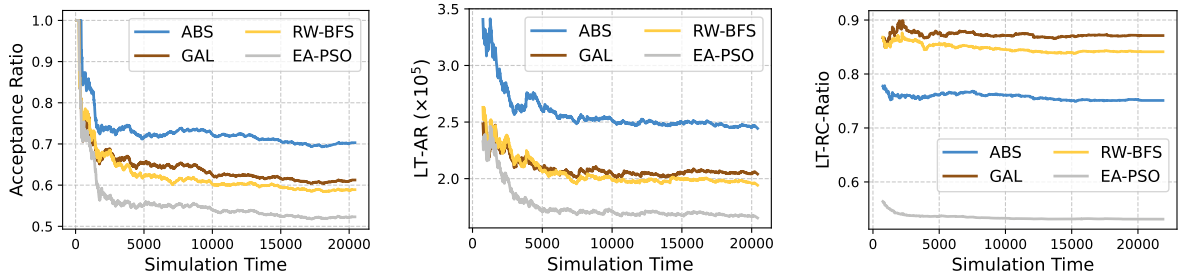
Unexpectedly, meta-heuristic algorithms EA-PSO and GA-STP, despite their strong global search capabilities, deliver only moderate results. Since both operate on independent node-level decisions and ignore the challenges introduced by SF co-location, their best performance merely approaches that of RW-BFS, rather than surpassing it.

2) Metric-based Analysis: A comparison and discussion of each performance metric is provided here.

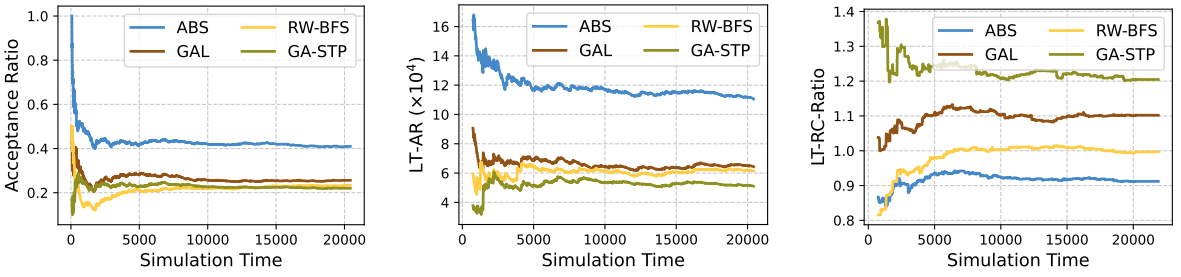
Acceptance ratio: It directly impacts user satisfaction, as frequent service denials can erode user patience. As shown in Tab. II, our ABS achieves significantly higher acceptance ratios than other algorithms, with improvements of at least 15% under the random topology and 60.2% under the real-world topology. However, the acceptance ratio alone has its limitations: it does not capture the quality of accepted requests. For example, given the same acceptance ratio, accepting a large number of requests with simple SEs may not lead to efficient resource utilization.

Revenue: This metric intuitively measures both the quantity and quality (complexity) of accepted requests, capturing the overall service gain. Higher revenue also indicates more efficient resource utilization of the algorithm, as it creates more value from limited resources. Therefore, combining revenue with acceptance ratio can provide a more comprehensive assessment of mapping quality. As shown in Tab. II, our ABS achieves at least an 18% and a 74.1% improvement in total revenue under random and real-world topologies, respectively. Notably, compared to GAL, ABS achieves a much greater improvement in total revenue than in acceptance ratio (e.g., 74.1% vs. 60.2% in the real-world topology). This significant gap further indicates that ABS is capable of accepting more complex and higher-value service requests, rather than merely increasing the number of accepted requests.

Long-term average revenue: It complements revenue by evaluating the ability to sustain high revenue throughout the simulation, reflecting long-term operational effectiveness rather than short-term bursts. Comparing the trends of acceptance ratio and long-term average revenue provides insights into the decision-making quality of different algorithms. Specifically, our ABS consistently exhibits a larger gap over other algorithms in long-term average revenue than in acceptance ratio, indicating a persistent preference for higher-quality requests. As a counterexample, in Figs. 5(a) and 5(b), although GAL achieves a higher acceptance ratio than RW-BFS after simulation time 5000, its long-term average revenue

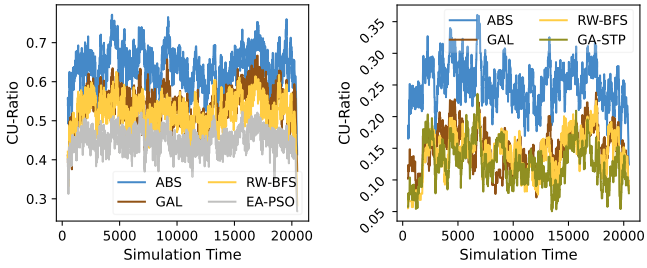


(a) Acceptance ratio (b) Long-term average revenue (c) Long-term revenue to cost ratio



(d) Acceptance ratio (e) Long-term average revenue (f) Long-term revenue to cost ratio

Fig. 5. Acceptance ratio, long-term average revenue, and long-term revenue to cost ratio over simulation time for the random topology (upper) and the real-world topology (lower) according to Tab. II. (All subsequent performance figures display only the best-performing algorithm from each category of solving methods.)



(a) Random topology (b) Real-world topology

Fig. 6. Computing resource utilization comparison over simulation time.

does not show a corresponding increase. Normally, if the value distribution of requests remains unchanged, a higher acceptance ratio should result in a higher average revenue. This suggests that GAL is accepting more small, less valuable requests during this period. A similar phenomenon can be observed in Figs. 5(d) and 5(e). These findings further validate, from a long-term operational perspective, that ABS's mapping decisions favor complex, high-value service requests, rather than simply maximizing the number of accepted requests.

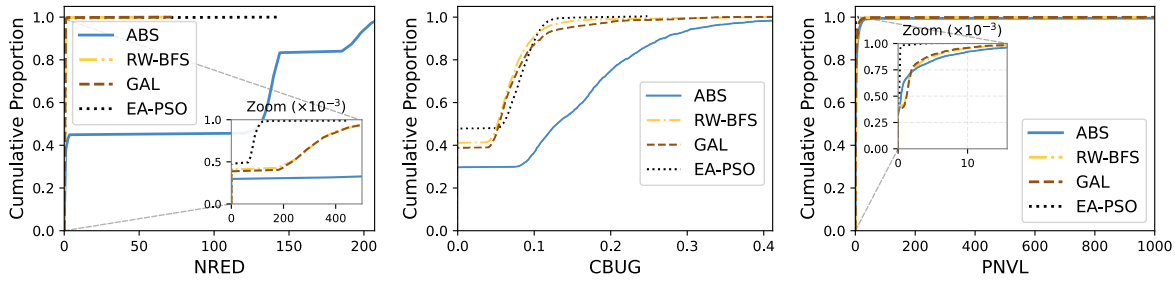
Profit: Tab. II presents the profit performance of each algorithm under the parameter settings ($\theta = 2$, $\omega = 0.5$), where ABS consistently demonstrates a significant advantage. It is essential to note that higher profits do not always require minimizing costs or maximizing the revenue-to-cost ratio. As long as costs are reasonable, prioritizing higher acceptance ratios and higher-quality requests can yield greater profit.

CN Resource Utilization: This metric directly reflects the effectiveness in integrating and utilizing distributed computing resources, which is the fundamental goal of CPN. Once the acceptance ratio stabilizes, it provides an intuitive measure of an algorithm's resource exploitation capability. As illustrated in Fig. 6, ABS achieves improvements of at least 19.3% and 73.2% over baseline algorithms under the two topologies, respectively. Notably, the consistency between CN resource utilization and revenue improvements mutually reinforces both metrics, highlighting that ABS's revenue advantage is fundamentally rooted in its superior exploitation of distributed computing resources. Accordingly, revenue becomes a meaningful indicator of CPN's core objective—maximizing resource utilization—which justifies our preference for maximizing revenue, even when it may involve higher costs.

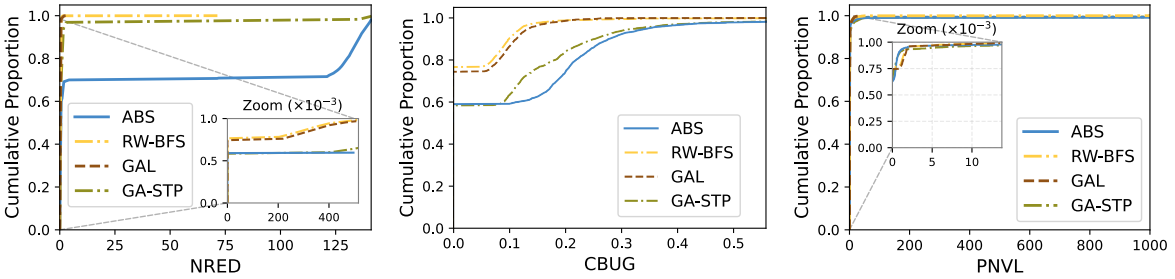
Revenue to Cost Ratio and Long-term Revenue to Cost Ratio: These metrics primarily reflect differences in network resource consumption when mapping SEs. Lower NL bandwidth usage for the same SE implies lower cost and higher RC-Ratios. However, in our work, maximizing computing resource utilization is the primary objective, with network bandwidth serving as the enabler rather than the end goal. Therefore, we are willing to tolerate higher network expenditure if it leads to greater acceptance ratios, revenues, and resource utilization; as such, a higher RC-Ratio is not always preferable. As shown in Tab. II and Figs. 5(c) and 5(f), although ABS is not optimal in terms of the RC-Ratio, its LT-RC-Ratio maintains a stable trend over time, without significant fluctuations. This steady trend demonstrates that the trade-off between network consumption and improved service gains, as well as computing resource utilization, is both rational and sustainable, reflecting ABS's well-balanced and reliable resource utilization strategy.

3) Extended Discussion: In the following, we further elaborate on two essential features of ABS.

A key advantage of our approach is its effective global search capability, which becomes especially important in network resource-constrained scenarios——a situation that may be commonly encountered in CPN environments. Both GAL



(a) Random topology



(b) Real-world topology

Fig. 7. CDF distributions of fragmentation evaluation metrics (NRED, CUBG, and PNVL) for 2,000 test requests' decisions: ABS versus each method's best-performing algorithm in the random topology (upper) and the real-world topology (lower).

and $\text{APSDPS}_{\text{init by RW-BFS}}$ build upon the solutions generated by RW-BFS and further improve performance by leveraging global search capabilities. For example, in the rocketfuel topology, where network resources are limited due to a higher number of CNs but fewer NLs (see Tab. I), GAL's global search increases revenue from 6.8% (RW-BFS) to 10.1%, a 48.5% improvement, while our $\text{APSDPS}_{\text{init by RW-BFS}}$ raises it from 21.9% to 67.6%, corresponding to a 208.7% relative improvement. These improvements are a direct result of compelling global exploration, and the much larger gain achieved by our method over GAL further demonstrates the superior global search capability of our approach.

Moreover, ABS incorporates an evaluation mechanism more closely aligned with actual performance than traditional network cost-based metrics. Existing search-based algorithms (e.g., EA-PSO, GA-STP, RL-QoS, GAL) mainly rely on revenue-to-cost ratios or equivalent metrics as guidance for decision-making. However, as shown in Tab.II, optimizing RC-Ratio does not correlate with revenue gains, indicating that this kind of local efficiency metric cannot capture system complexity or predict actual performance in CPN. In contrast, our fragmentation-based metrics more accurately reflect global resource utilization, with higher values indicating lower fragmentation and higher efficiency. The CDF analysis in Fig.7 shows that ABS predominantly achieves optimal metric concentrations across topologies, outperforming the top baselines and validating that our metrics reliably indicate and promote superior global performance. Additionally, the degree of separation between the CDF curves of NRED, CUBG, and PNVL highlights their differing associations with overall performance. Specifically, NRED shows the strongest correlation, followed by CUBG, while PNVL has the least. This suggests a natural weighting hierarchy among these metrics when evaluating decision quality. Therefore, in practical applications, higher weights should be assigned to metrics more strongly correlated with overall performance.

VI. Conclusion

In this paper, we have conducted a formal study of the service entity mapping problem in CPN environments, targeting optimal service-to-infrastructure assignment that fully leverages network-enabled computing resource integration. We have formally defined the problem, proved its theoretical intractability, and highlighted key practical challenges, including variable coupling, solution space explosion, and the need for global performance guidance. We have proposed the ABS approach—a modular and adaptive search framework, instantiated in this work with a distributed particle swarm optimizer. ABS introduces graph partitioning-based reformulation, bilevel optimization, and fragmentation-aware evaluation to address the identified challenges effectively. Extensive simulations across diverse CPN scenarios demonstrate that ABS achieves significant and sustained improvements over state-of-the-art methods across key performance metrics and confirm the effectiveness of the fragmentation-based evaluation mechanism. In future work, we will leverage the modular design of ABS to explore advanced search strategies (e.g., DRL) and incorporate additional CPN scenario features, such as resource multidimensionality and heterogeneity.

References

[1] W. Zhang *et al.*, "(com)2net: A novel communication and computation integrated network architecture," *IEEE Network*, vol. 38, no. 2, pp. 35–44, 2024.

[2] T. Dong *et al.*, "Standing on the shoulders of giants: Cross-slice federated meta learning for resource orchestration to cold-start slice," *IEEE/ACM Transactions on Networking*, vol. 31, no. 2, pp. 828–845, 2022.

[3] Z. Hong *et al.*, "Intelligence-endogenous management platform for computing and network convergence," *IEEE Network*, vol. 38, no. 4, pp. 166–173, 2023.

[4] W. Zhang *et al.*, "Dynamic resource scheduling for deterministic communication, computation, and control integration in industrial cyber-physical systems," *IEEE Transactions on Cognitive Communications and Networking*, 2025, early access, May 15.

[5] S. Deng *et al.*, "Cloud-native computing: A survey from the perspective of services," *Proceedings of the IEEE*, vol. 112, no. 1, pp. 12–46, 2024.

[6] L. Wang *et al.*, "Service entity placement for social virtual reality applications in edge computing," in *2018 IEEE Conference on Computer Communications (IEEE INFOCOM 2018)*. IEEE, 2018, pp. 468–476.

[7] J. He *et al.*, "Service-oriented network resource orchestration in space-air-ground integrated network," *IEEE Transactions on Vehicular Technology*, vol. 73, no. 1, pp. 1162–1174, 2023.

[8] I. Taleb *et al.*, "A survey on services placement algorithms in integrated cloud-fog/edge computing," *ACM Computing Surveys*, vol. 57, no. 11, pp. 1–36, 2025.

[9] X. Fan *et al.*, "Qoe-oriented dependent task scheduling under multi-dimensional qos constraints over distributed networks," *IEEE Transactions on Network and Service Management*, vol. 22, no. 1, pp. 516–531, 2024.

[10] M. Goudarzi *et al.*, "A distributed deep reinforcement learning technique for application placement in edge and fog computing environments," *IEEE Transactions on Mobile Computing*, vol. 22, no. 5, pp. 2491–2505, 2021.

[11] R. Wang *et al.*, "Efficient deployment of partial parallelized service function chains in cpu+dpu-based heterogeneous nfv platforms," *IEEE Transactions on Mobile Computing*, vol. 23, no. 10, pp. 9090–9107, 2024.

[12] X. Zhang *et al.*, "Monte: Sfcs migration scheme in the distributed programmable data plane," *IEEE Transactions on Parallel and Distributed Systems*, vol. 36, no. 4, pp. 633–644, 2025.

[13] P. Zhang *et al.*, "Energy aware space-air-ground integrated network resource orchestration algorithm," *IEEE Transactions on Vehicular Technology*, vol. 73, no. 12, pp. 18 950–18 960, 2024.

[14] Y. Zhang *et al.*, "Qos aware virtual network embedding in space-air-ground-ocean integrated network," *IEEE Transactions on Services Computing*, vol. 17, no. 4, pp. 1712–1723, 2024.

[15] S. Wu *et al.*, "Ai-empowered virtual network embedding: a comprehensive survey," *IEEE Communications Surveys & Tutorials*, vol. 27, no. 2, pp. 1395–1426, 2024.

[16] W. Fan *et al.*, "Node essentiality assessment and distributed collaborative virtual network embedding in datacenters," *IEEE Transactions on Parallel and Distributed Systems*, vol. 34, no. 4, pp. 1265–1280, 2023.

[17] Y. Tan *et al.*, "5g end-to-end slice embedding based on heterogeneous graph neural network and reinforcement learning," *IEEE Transactions on Cognitive Communications and Networking*, vol. 10, no. 3, pp. 1119–1131, 2024.

[18] D. G. Andersen, "Theoretical approaches to node assignment," Carnegie Mellon University, Tech. Rep., Dec. 2002, [Online]. Available: http://repository.cmu.edu/compsci/86/.

[19] W. Zhang *et al.*, "Repeatable multi-dimensional virtual network embedding in cloud service platform," *IEEE Transactions on Services Computing*, vol. 15, no. 6, pp. 3499–3512, 2022.

[20] N. M. K. Chowdhury *et al.*, "A survey of network virtualization," *Computer Networks*, vol. 54, no. 5, pp. 862–876, 2010.

[21] T. Ma *et al.*, "Klonet: an {Easy-to-Use} and scalable platform for computer networks education," in *21st USENIX Symposium on Networked Systems Design and Implementation (USENIX NSDI 24)*, 2024, pp. 2025–2046.

[22] Q. Weng *et al.*, "Beware of fragmentation: Scheduling {GPU-Sharing} workloads with fragmentation gradient descent," in *2023 USENIX Annual Technical Conference (USENIX ATC 23)*, 2023, pp. 995–1008.

[23] C. Miao *et al.*, "Megate: Extending wan traffic engineering to millions of endpoints in virtualized cloud," in *Proceedings of the ACM SIGCOMM 2024 Conference*, 2024, pp. 103–116.

[24] Y. Zhang *et al.*, "Service function chain deployment with vnf-dependent software migration in multi-domain networks," *IEEE Transactions on Mobile Computing*, vol. 24, no. 5, pp. 3685–3702, 2024.

[25] H. Geng *et al.*, "Gal-vne: Solving the vne problem with global reinforcement learning and local one-shot neural prediction," in *Proceedings of the 29th ACM SIGKDD Conference on Knowledge Discovery and Data Mining*, 2023, pp. 531–543.

[26] Y. Guan *et al.*, "Multidimensional resource fragmentation-aware virtual network embedding for iot applications in mec networks," *IEEE Internet of Things Journal*, vol. 10, no. 24, pp. 22 223–22 232, 2023.

[27] S. Chen *et al.*, "Graph neural network aided deep reinforcement learning for microservice deployment in cooperative edge computing," *IEEE Transactions on Services Computing*, vol. 17, no. 6, pp. 3742–3757, 2024.

[28] A. Song *et al.*, "A divide-and-conquer evolutionary algorithm for large-scale virtual network embedding," *IEEE Transactions on Evolutionary Computation*, vol. 24, no. 3, pp. 566–580, 2019.

[29] K. Nguyen *et al.*, "Toward adaptive joint node and link mapping algorithms for embedding virtual networks: A conciliation strategy," *IEEE Transactions on Network and Service Management*, vol. 19, no. 3, pp. 3323–3340, 2022.

[30] L. Gong, H. Jiang, Y. Wang, and Z. Zhu, "Novel location-constrained virtual network embedding lc-vne algorithms towards integrated node and link mapping," *IEEE/ACM Transactions on Networking*, vol. 24, no. 6, pp. 3648–3661, 2016.

[31] G. Karypis *et al.*, "Metis: A software package for partitioning unstructured graphs, partitioning meshes, and computing fill-reducing orderings of sparse matrices," University of Minnesota, Tech. Rep., Jun. 2002, [Online]. Available: https://hdl.handle.net/11299/215346.

[32] K. Salimifard *et al.*, "The multicommodity network flow problem: state of the art classification, applications, and solution methods," *Operational Research*, vol. 22, no. 1, pp. 1–47, 2022.

[33] A. Sinha *et al.*, "A review on bilevel optimization: From classical to evolutionary approaches and applications," *IEEE transactions on evolutionary computation*, vol. 22, no. 2, pp. 276–295, 2017.

[34] K. Andreev *et al.*, "Balanced graph partitioning," in *Proceedings of the sixteenth annual ACM symposium on Parallelism in algorithms and architectures*, 2004, pp. 120–124.

[35] Q. Yang *et al.*, "A distributed swarm optimizer with adaptive communication for large-scale optimization," *IEEE transactions on cybernetics*, vol. 50, no. 7, pp. 3393–3408, 2019.

[36] Y. Shi *et al.*, "A modified particle swarm optimizer," in *1998 IEEE international conference on evolutionary computation proceedings*, 1998, pp. 69–73.

[37] X. Cheng *et al.*, "Virtual network embedding through topology-aware node ranking," *ACM SIGCOMM Computer Communication Review*, vol. 41, no. 2, pp. 38–47, 2011.

[38] S. Su *et al.*, "Energy-aware virtual network embedding," *IEEE/ACM Transactions on Networking*, vol. 22, no. 5, pp. 1607–1620, 2014.

[39] N. Spring *et al.*, "Measuring isp topologies with rocketfuel," *ACM SIGCOMM Computer Communication Review*, vol. 32, no. 4, pp. 133–145, 2002.

APPENDIX A
PROOFS OF THEORETICAL RESULTS

Theorem 2. *($\mathbb{P}3$) and ($\mathbb{P}4$) are equivalent.*

Proof. Assume that $\mathbf{x}$ is an arbitrary feasible solution to the problem ($\mathbb{P}3$). Then, we construct $\boldsymbol{\rho}$ as:

$$\forall m^s \in N^s: \quad \rho_{m^s} = \frac{\sum_{u^v \in N_i^v} c(u^v) x_{m^s}^{u^v}}{\sum_{u^v \in N_i^v} c(u^v)}. \tag{27}$$

Given a feasible solution $\mathbf{x}$ to ($\mathbb{P}3$), after constructing $\boldsymbol{\rho}$ as described above, all additional constraints (14c)-(14e) are evidently satisfied. Thus, we can obtain a feasible solution $(\boldsymbol{\rho}, \mathbf{x})$ in ($\mathbb{P}4$).

Then, given an arbitrary feasible solution $(\boldsymbol{\rho}, \mathbf{x})$ to the problem ($\mathbb{P}4$), the resulted $\mathbf{x}$ by eliminating the variable $\boldsymbol{\rho}$ is obviously a feasible solution to ($\mathbb{P}3$).

Moreover, the objective functions of ($\mathbb{P}3$) and ($\mathbb{P}4$) are exactly the same and depend solely on $\mathbf{x}$. Thus, if $(\boldsymbol{\rho}^*, \mathbf{x}^*)$ achieves the optimal objective value of ($\mathbb{P}4$), then $\mathbf{x}^*$ is also the optimal solution to ($\mathbb{P}3$), and vice versa.

In conclusion, each feasible solution set is in one-to-one correspondence via the mapping above, and they share the same objective function in terms of $\mathbf{x}$. ■

Theorem 3. *The PW-kGPP problem is NP-Hard.*

Proof. The balanced graph partitioning (BGP) problem is a known problem [34]: given a graph $G = (V, E)$ and an integer $k \geq 2$, the task is to partition the vertex set V into k disjoint subsets $V_1, V_2, ..., V_k$ such that: the size of each subset satisfies $|V_p| \leq \lceil |V|/k \rceil for\, p = 1, 2, ..., k$ and the cut weight is minimized. It is very easy to map any BGP instance to a PW-kGPP instance, proceeding as follows: assign a weight of $w_n = 1$ to each vertex in V, define the proportion for each subset as $r_p = 1/k$ for all subsets V_p, and use a tolerance coefficient $\theta = 0$. Thus, any problem belonging to BGP can be solved by an algorithm designed for PW-kGPP; that is, BGP can be reduced to PW-kGPP. Since BGP is NP-Hard, PW-kGPP is also NP-Hard. ■

Corollary 2. *($\mathbb{P}4$) is NP-Hard.*

Proof. According to the above analysis, a polynomial-time reduction exists that transforms any instance of PW-kGPP into an instance of ($\mathbb{P}4$). According to Theorem 2, it can be proved that ($\mathbb{P}4$) is NP-Hard. ■

Corollary 3. *($\mathbb{P}3$) is NP-Hard.*

Proof. Combining Theorem 2 and Corollary 2, ($\mathbb{P}3$) can be easily proved to be NP-Hard. ■

Lemma 1. *The optimal solutions to ($\mathbb{P}4$) are feasible solutions to ($\mathbb{P}4 - BOP$).*

Proof. Let $(\boldsymbol{\rho}^*, \mathbf{x}^*)$ be a global optimal solution to ($\mathbb{P}4$). That is to say, $\boldsymbol{\rho}^*$ satisfies $\sum \rho_{m^s}^* = 1$ and $\rho_{m^s}^* \geq 0$, complying with upper-level constraints in ($\mathbb{P}4 - BOP$); and $\mathbf{x}^*$ satisfies all lower-level constraints for the given $\boldsymbol{\rho}^*$. Then, $(\boldsymbol{\rho}^*, \mathbf{x}^*)$ is a feasible solution to ($\mathbb{P}4 - BOP$). ■

Lemma 2. *The optimal solutions to ($\mathbb{P}4 - BOP$) are feasible solutions to ($\mathbb{P}4$).*

Proof. Let $(\boldsymbol{\rho}^\dagger, \mathbf{x}^\dagger)$ be a global optimal solution to ($\mathbb{P}4 - BOP$). By definition of ($\mathbb{P}4 - BOP$), $(\boldsymbol{\rho}^\dagger, \mathbf{x}^\dagger)$ satisfies all constraints in ($\mathbb{P}4$), making it a feasible solution. ■

Theorem 4. *($\mathbb{P}4 - BOP$) and ($\mathbb{P}4$) are equivalent.*

Proof. Following from Lemmas 1 and 2, they possess the feasible set equivalence. Since both problems share the same objective function, their objects are consistent. Then, the original problem ($\mathbb{P}4$) and its BOP form ($\mathbb{P}4 - BOP$) share identical feasible sets and optimal solutions. ■

Proposition 1. *Suppose the outer layer can traverse all possible values of ρ_{m^s}, and the inner layer will accurately solve the corresponding problems. The final solution obtained by the nested approach will be the optimal one for ($\mathbb{P}2$).*

Proof. Suppose, for contradiction, that the nested approach does not yield the optimal solution to ($\mathbb{P}2$). Let $(\boldsymbol{\rho}^*, \mathbf{x}^*, \mathbf{f}^*)$ be an optimal solution. Since the outer layer exhaustively traverses all possible $\boldsymbol{\rho}$, it will consider $\boldsymbol{\rho}^*$. For this choice, the inner layer solves the corresponding PW-kGPP and IMCF problems optimally, yielding the minimum bandwidth resource cost for $\boldsymbol{\rho}^*$. Therefore, the assumption is contradicted. ■

APPENDIX B
DETAILS OF DEFINITION 1

Definition 1 (Proportional Weight-Constrained k-way Graph Partitioning Problem, PW-kGPP)**.**

$$\text{PW}-\text{kGPP}: \min_{x_p^i} \sum_{(i,j)\in E} c_{ij} \sum_{p=1}^{k} x_p^i (1 - x_p^j) \tag{28a}$$

$$s.t. \quad \forall p \in \{1, 2, ..., k\}:$$

$$(1-\theta) r_p \leq \frac{\sum_{i \in V_p} w_i}{\sum_{i \in V} w_i} \leq (1+\theta) r_p, \tag{28b}$$

where θ is a configurable tolerance coefficient.

APPENDIX C
SUPPLEMENTAL MATERIALS FOR ABS IMPLEMENTATION

A. Pseudocode for Algorithms 1 to 4

The pseudocode can be found in Algorithms 1, 2, 3, 4.

B. Details of Time Complexity Analysis

In practical scenarios, the most time-consuming component of the algorithm is the iterative process executed by the workers (Algorithm 3), which forms the basis of our complexity analysis. During initialization (Algorithm 4), the *init_solver* and *kshortestpath* functions are invoked $|N_S|$ times. The dominant complexity in *init_solver* arises from the *metispartition* function. Consequently, the overall complexity of this phase is: $\mathcal{O}(|N_S| \cdot (|L^s| + k \cdot |N^s| \cdot (|L^s| + |N^s| \log |N^s|)))$. In the iterative main body, the algorithm performs ITR_{max} iterations. For each iteration, the swarm evolutionary update (Algorithm 2) processes $|N_S|$ particles. The most time-consuming operations

Algorithm 1: ABS

Input: G_i^v, G^s, Worker Number N_W
Output: Best SEM Solution $(\mathbf{x}^*, \mathbf{f}^*)$

Set archive capacity N_A, counter $c_{terminate} = 0$;
Initialize the set of communication connections **conns** with N_W $conns$ and archive $\mathbf{A} \leftarrow \emptyset$;
Invoke Algorithm 3 given G_i^v and G^s as input to activate N_W workers, and assign each of them a $conn \in$ **conns**;
while $c_{terminate} \neq N_W$ **do**
  for $conn \in$ **conns** **do**
    if *conn.has_data()* **then**
      $(info, particle) \leftarrow$ conn.receive();
      switch $info$ **do**
        case *'best_particle'* **do**
          if $|\mathbf{A}| < N_A$ **then**
            Add $particle$ to $\mathbf{A}$;
          else
            Replace random $\mathbf{A}[r]$ if $\mathcal{F}(particle.solution) < \mathcal{F}(\mathbf{A}[r].solution)$;
        case *'newP_request'* **do**
          conn.send($\mathbf{A}$[rand($|\mathbf{A}|$)]);
        case *'terminate'* **do**
          $c_{terminate} \leftarrow c_{terminate} + 1$;
return $\text{argmin}_{particle \in \mathbf{A}} \mathcal{F}(particle.solution)$;

Algorithm 2: Swarm Evolutionary Update

Input: G_i^v, G^s, Elite Set $\mathbf{ES}^{iter}$, Common Set **CS**, Local Archive **LA**
Output: Updated common set **CS**

for $particle \in$ **CS** **do**
  if $iter == 1$ **then**
    Set $particle.dimension$ as the number of elements in $particle.position$;
  Set $r_position = [0] * particle.position$.len();
  Get $temp_position$ for $particle$ using (23)-(26);
  $particle.position = [max(0, \rho)\ for\ \rho\ in\ temp_position]$;
  Find the $particle.dimension$ largest elements of $particle.position$, normalize them, and set them into their corresponding positions in $r_position$;
  $\mathbf{x}' \leftarrow metispartition(\cdot)$, $\mathbf{f}' \leftarrow kshortestpath(\cdot)$;
  if $(\mathbf{x}', \mathbf{f}')$ *satisfies (1)-(6)* **then**
    $particle.dimension =$ max(1, $particle.dimension - 1$)

Algorithm 3: ABS Iteration Worker

Input: G_i^v, G^s, Communication Connection $conn$

Set swarm size N_S, max iteration times ITR_{max}, elite set capacity N_E, local archive capacity N_{LA}, particle with global best fitness $gbest = \{\}$;
Initialize the beginning elite set $\mathbf{ES}^0 \leftarrow \emptyset$, common set **CS** $\leftarrow \emptyset$, and local archive **LA** $\leftarrow \emptyset$;
Invoke Algorithm 4 given G_i^v, G^s, and N_S as input to get initial **Particles**;
for $iter = 1$ **to** ITR_{max} **do**
  Compute the fitness value $\mathcal{F}(particle.solution)$ for $particle \in$ **Particles**;
  Sort **Particles** by fitness values, update $gbest$, and put N_E best particles into $\mathbf{ES}^{iter}$ and $(N_S - N_E)$ worst $particles$ into **CS**;
  if $gbest$ *is updated* **then**
    $conn$.send(*'best_particle'*, $gbest$);
  if $\mathbf{ES}^{iter} == \mathbf{ES}^{iter-1}$ **then**
    $conn$.send(*'newP_request'*);
    $n_particle$ = $conn$.receive();
    if $\mathbf{LA}$.*len()* $< N_{LA}$ **then**
      Add $n_particle$ to **LA**;
    else
      Replace the worst particle $w_particle \in$ **LA** with $n_particle$, if $\mathcal{F}(n_particle.solution)$ is smaller;
  Invoke Algorithm 2 given **CS**, $\mathbf{ES}^{iter}$, and **LA** as input to make $particle \in$ **CS** evolve;
  $iter = iter + 1$;
$conn$.send(*'terminate'*);

for each particle are those invocations of the *metispartition* and *kshortestpath* functions. Therefore, the complexity of this phase is: $\mathcal{O}(ITR_{max} \cdot |N_S| \cdot (|L^s| + k \cdot |N^s| \cdot (|L^s| + |N^s| \log |N^s|)))$. By combining the complexities of the two phases, the overall complexity of the algorithm executed by each worker can be simplified as: $\mathcal{O}(ITR_{max} \cdot |N_S| \cdot k \cdot |N^s| \cdot (|L^s| + |N^s| \log |N^s|)$.

APPENDIX D
EXPERIMENTAL DETAILS

A. Compared Methods

Heuristc–

- **RW-BFS** [37] is a classic rank-based heuristic considering CPN topology and ranking each CN via random walk. The SF mapping and correlated LL mapping are conducted simultaneously based on the node rank by breadth-first searching (BFS).
- **RMD** [19] introduces a service entity topology preprocessing technology and uses a heuristic strategy for mapping, which achieves a topology-aware solution through graph coarsening, partitioning, uncoarsening, and merging nodes with strong link relations.

Meta-heuristic–

- **EA-PSO** [38] is a classic meta-heuristic that adopts a discrete PSO algorithm for directly searching the SF mapping solution, along with the shortest path algorithm to map the related LLs.
- **GA-STP** [29] relies on Genetic Algorithm (GA) to jointly coordinates SF and LL mappings. Meanwhile, a novel heuristic conciliation mechanism is embedded in the exploration process of the GA algorithm to handle a set of potentially infeasible LL mapping solutions.

Learning-based–

- **RL-QoS** [14] is a model-free reinforcement learning algorithm that leverages a policy gradient method with a convolutional neural network (CNN) and softmax layers to make node decisions based on historical data. It estimates the policy network through the CNN and updates the gradient using the policy gradient algorithm.
- **GAL** [25] employs a two-stage framework: initially, a graph neural network is trained with supervised learning to emulate classic node ranking (e.g., RW-BFS), followed by reinforcement learning for further improvement, with final SF and LL mapping performed using a BFS strategy.

B. Evaluation Metrics

Denote $\Upsilon(t)$ as the set of all arrived SE topologies and $\Upsilon^a(t)$ as the subset of successfully mapped ones.

- **Acceptance ratio:** This metric is formulated in (29), and it directly reflects the proportion of service entities successfully mapped by the algorithm.

$$p_{ac}(t) = \frac{|\Upsilon^a(t)|}{|\Upsilon(t)|} \tag{29}$$

- **Revenue:** This metric reflects the total revenue generated by all successfully accepted service requests at a given time t. (30) shows the formula.

$$\sum_{G_i^v \in \Upsilon^a(t)} \mathcal{R}(G_i^v) \tag{30}$$

Algorithm 4: Particle Swarm Initializing

Input: G_i^v, G^s, Swarm Size N_S
Output: Particle Swarm **Particles**

Initialize **Particles** $\leftarrow \emptyset$ and $\boldsymbol{\rho}, \mathbf{x}, \mathbf{f} \leftarrow None$;
for $i = 1$ **to** N_S **do**
  $(\boldsymbol{\rho}, \mathbf{x}) \leftarrow$ *init_solver*(G_i^v, G^s);
  $\mathbf{f} \leftarrow$ *kshortestpath*(G_i^v, G^s, $\mathbf{x}$);
  Add particle($\boldsymbol{\rho}$, ($\mathbf{x}, \mathbf{f}$)) to **Particles**;
return Particles;
//
Function `init_solver`(G_i^v, G^s)**:**
  Set $max_depth, depth = 0$; $\boldsymbol{\rho}, \mathbf{x} \leftarrow None$;
  Initialize the chosen CN set, current neighbor set, next neighbor set, and useless neighbor set: **chosen**, **cNBR**, **nNBR**, **uNBR** $\leftarrow \emptyset$;
  Select m^s with $C(m^s) > 0$ by resource-weighted randomization; update **chosen** and **cNBR**;
  while chosen.*size()* $< min(|N^s|, |N_i^v|)$ ***and*** $depth \leq max_depth$ **do**
    if cNBR $\neq \emptyset$ **then**
      Select m^s from **cNBR** via resource-weighted randomization, add it to **chosen**, remove it from **cNBR**;
      For each neighbor of m^s, if it is not in **chosen**, add it to **nNBR** if it has non-zero resources; otherwise, add it to **uNBR**;
      Calculate ρ_{m^s} as: $\forall m^s \in$ **chosen**, $\rho_{m^s} = C(m^s)/\sum_{m^s \in \textbf{chosen}} C(m_i^s)$, set $\rho_{m^s} = 0$ for $m^s \notin$ **chosen**, and update $\boldsymbol{\rho}$;
      $\mathbf{x}' \leftarrow$ *metispartition*(G_i^v, $\boldsymbol{\rho}$);
      if $\mathbf{x}'$ *satisfies constraints (1)-(3)* **then**
        set $\mathbf{x} = \mathbf{x}'$; **break**
    else
      if nNBR $\neq \emptyset$ **then**
        Set **cNBR** as **nNBR**, **nNBR** $\leftarrow \emptyset$, and **uNBR** $\leftarrow \emptyset$;
      else if uNBR $\neq \emptyset$ **then**
        Copy **uNBR** to **uNBR**$'$ and set **nNBR**, **uNBR** $\leftarrow \emptyset$;
        For each neighbor of $m^s \in$ **uNBR**$'$, if it is not in **chosen**, add it to **nNBR** if it has non-zero resources; otherwise, add it to **uNBR**;
        $max_depth = max_depth + 1$;
      else
        break;
  return ($\boldsymbol{\rho}, \mathbf{x}$);

- **Long-term average revenue (LT-AR):** It complements the total revenue, measuring the ability of the algorithm to generate revenue throughout the simulation period continuously[5]. This metric is expressed in (31):

$$\lim_{T\to\infty} \frac{\sum_{t=0}^{T} \mathcal{R}(G^v(t))}{T} \tag{31}$$

- **Profit:** It is formulated in (32). This metric integrates revenue, acceptance ratio, and cost to comprehensively evaluate the practical value of the algorithm, reflecting both the efficient utilization of computing resources and the overall service satisfaction.

$$(p_{ac}(t))^{\theta} \cdot \Big(\sum_{G_i^v \in \Upsilon^a(t)} \mathcal{R}(G_i^v) - \omega \cdot \sum_{G_i^v \in \Upsilon^a(t)} \mathcal{C}(G_i^v) \Big), \tag{32}$$

  where $\theta \geq 1$ is a configurable weighting coefficient that adjusts the relative importance of the service acceptance ratio for the system's achieved profit; and $0 < \omega < 1$ serves as a tunable weighting factor that determines the system's willingness to trade additional network resource consumption for higher computing resource utilization.

[5]Rather than infinite time horizons, we approximate these long-term metrics by cumulative metrics at the simulation time of the last arrival request.

- **CN Resource Utilization (CU-Ratio):** This metric indicates the overall utilization of CNs within the CPN topology by service workloads at a given time t. It represents the ratio of the total CPU resources utilized by all currently accepted service requests at a specific time to the total initial CPU capacity available across all CNs, which is expressed in (33):

$$\frac{\sum_{m^s \in N^s} U_C(m^s, t)}{\sum_{m^s \in N^s} C_{init}(m^s)}, \tag{33}$$

  where $U_C(m^s, t)$ is the instantaneous CPU resource usage of CN m^s at a timestamp t, and $C_{init}(m^s)$ denotes the initial CPU capacity of the corresponding node.
- **Revenue to cost ratio (RC-Ratio):** This metric quantifies the efficiency of mapping decisions by measuring the ratio between the cumulative revenue and cost of all accepted requests at time t, as shown in (34).

$$\frac{\sum_{G_i^v \in \Upsilon^a(t)} \mathcal{R}(G_i^v)}{\sum_{G_i^v \in \Upsilon^a(t)} \mathcal{C}(G_i^v)} \tag{34}$$

  We do not use cost alone as a performance metric because, by definition, although it reflects the overhead of LLnM, higher cost often indicates that more services have been mapped. Therefore, cost alone does not meaningfully reflect algorithm efficiency. Instead, the RC-ratio better captures bandwidth usage efficiency by relating total revenue to total cost.
- **Long-term revenue to cost ratio (LT-RC-Ratio):** It calculates the ratio of long-term average revenue and cost generated during the service provisioning process.The formula is shown in (35).

$$\lim_{T\to\infty} \frac{\sum_{t=0}^{T} \mathcal{R}(G^v(t))}{\sum_{t=0}^{T} \mathcal{C}(G^v(t))} \tag{35}$$